Boundary-Layer Meteorol (2013) 147:369–400
DOI 10.1007/s10546-012-9796-4

ARTICLE

Turbulence in Sparse, Organized Vegetative Canopies: A Large-Eddy Simulation Study

Brian N. Bailey · Rob Stoll

Received: 7 August 2012 / Accepted: 24 December 2012 / Published online: 16 January 2013

Abstract A large-eddy simulation study was performed to characterize turbulence in sparse, row-oriented canopies. This was accomplished by simulating a set of heterogeneous row-oriented canopies with varying row vegetation density and spacing. To determine the effects of heterogeneity, results were compared to horizontally homogeneous canopies with an equivalent 'effective' leaf area index. By using a proper effective leaf area index, plane-averaged mean velocities and bulk scaling parameters contained only small errors when heterogeneity was ignored. However, many cases had significantly larger second- and third-order velocity moments in the presence of heterogeneity. Some heterogeneous canopies also contained dispersive fluxes in the lower canopy that were over 20 % as large as the turbulent flux. Impacts of heterogeneity were most pronounced in the cases of large row leaf area density and widely spaced rows. Despite the substantial amount of open space in the sparse canopies, vertical velocity skewness and quadrant-hole analysis indicated that the flow behaved predominantly as a canopy layer even though integral length scales at the canopy top no longer followed mixing-layer scaling. This was supported by the fact that similar composite-averaged coherent structures could be readily identified in both the heterogeneous and homogeneous canopies. Heterogeneity had an effect on coherent structures, in that structure detection events were most likely to occur just upwind of the vegetation rows. In simulations with large row spacing, these structures also penetrated deeper into the canopy when compared to the equivalent homogeneous canopy.

Keywords Dispersive flux · Large-eddy simulation · Sparse canopy · Vineyard

B. N. Bailey · R. Stoll (✉)
Department of Mechanical Engineering, University of Utah, Salt Lake City, UT, USA
e-mail: rstoll@eng.utah.edu

B. N. Bailey
e-mail: bbailey@eng.utah.edu

1 Introduction

The exchange of momentum between the atmosphere and vegetative canopies plays an important role in many atmospheric processes. Near the land surface, the presence of the canopy has a strong influence on the transport of momentum, heat, moisture, and the distribution and concentration of particles and pollutants. The density of canopies plays a critical role in the characteristics of these transport processes in and above the canopy (Finnigan 2000; Poggi et al. 2004a; Dupont and Brunet 2008; Huang et al. 2009).

Many researchers have studied momentum and scalar transport in crop and forest canopies grown in dense arrangements where the mean spacing between individual plants is smaller than the plant height (e.g., Finnigan 2000; Cescatti and Marcolla 2004; Poggi et al. 2004a,b; van Hout 2007; Thomas and Foken 2007; Yi 2007; Cava and Katul 2008; Dupont and Brunet 2008; Finnigan et al. 2009). Similarly, windbreak/shelterbelt flows where canopy elements are effectively isolated have also received considerable attention (e.g., Wilson 1985; Wang and Takle 1995; Judd et al. 1996; Patton et al. 1998). However, many perennial crops are grown in moderately sparse, row-oriented arrangements, the classical example being a grapevine canopy. These types of canopies lie in an intermediate range between dense canopy arrangements and isolated windbreaks. Increasingly, many perennial crops traditionally grown in dense canopy arrangements are undergoing transition to sparse, row-oriented canopies (Lauri 2009; Talaie et al. 2011). This has been driven by recognition of the benefits of increased sun exposure (e.g., Tarara et al. 2005) as well as current and future interest in mechanized harvesting methods. In addition, many row-oriented annual crop canopies that are dense when mature are sparse early in their growth cycle (e.g., corn, tomatoes). In forestry systems, selective logging practices can also result in sparse canopies (Novak et al. 2000). Despite the prevalence and importance of sparse canopies, relatively little is known about how the architecture of these canopies affects the transport of momentum and scalars in and above them. This information is critical towards improving the understanding of how canopy drag on plants is affected by canopy architecture, how pollen and airborne plant pathogens move through canopies, and how canopy architecture affects the transport of heat, water vapour, and carbon dioxide.

Past studies of flow dynamics in dense canopies have identified important features that dominate the production and dissipation of energy: highly coherent turbulent motions with length scales on the order of the canopy height that appear to dominate turbulent fluxes near the canopy (Finnigan 2000), and short-circuiting of the turbulent energy cascade in the canopy due to small-scale canopy element vortex shedding (Poggi et al. 2004b; van Hout 2007; Cava and Katul 2008). These features combine in a non-linear way, resulting in high turbulence intensities and intermittency that contribute to a generally poor understanding of the link between small-scale and large-scale flow features (Poggi et al. 2004b). The mixing-layer analogy has been a particularly popular explanation for the intermittency of canopy turbulence and the existence of canopy-scale coherent structures (Raupach et al. 1996; Finnigan 2000; Finnigan et al. 2009). Experimental and numerical studies have concluded that this analogy breaks down when the canopy density falls below a critical value (Novak et al. 2000; Dupont and Brunet 2008; Huang et al. 2009). One explanation given for this is that the canopy flow undergoes transition from a mixing-layer dominated flow to a rough-wall boundary-layer dominated flow (Huang et al. 2009). A second related explanation based on experimental data is that, as canopy density decreases, the spacing between canopy elements (e.g., trees) becomes more important (Novak et al. 2000). These explanations have remained mostly conceptual and have yet to address the role of canopy organization (i.e., specific geometry). Instead, the focus of studies examining canopy density has either

been on simulations of continuous, horizontally homogeneous canopies (Dupont and Brunet 2008; Huang et al. 2009) or wind-tunnel and water-channel studies of closely spaced arrays of cylinders (Novak et al. 2000; Poggi et al. 2004a). All these studies demonstrated a clear dependence of turbulence statistics on canopy density. The experimental studies (Novak et al. 2000; Poggi et al. 2004a) also found evidence of a direct impact of horizontal canopy geometry on flow dynamics. Novak et al. (2000) showed that turbulent integral length scales in the canopy have a dependence on the spacing between canopy elements. Poggi et al. (2004a) found an increase in spectral energy at length scales corresponding to the element diameter, which they associated with spectral short circuiting. The numerical studies examining canopy density effects represented the canopy as horizontally homogeneous, therefore, they did not include any possible effects of horizontal canopy heterogeneity. Some numerical studies have indicated an importance of representing horizontal canopy geometry (Yue et al. 2007; Bohrer et al. 2009; Schlegel et al. 2012). The study of Bohrer et al. (2009) demonstrated that randomly distributed tree-scale heterogeneity affects mean canopy flow scaling parameters and the structure of the canopy velocity field in the canopy roughness sublayer.

In windbreak/shelterbelt flows, the effects of an individual plant structure are localized to the region near the windbreak. These flows are commonly characterized by an upwind freestream region, a region in which the flow field is modified from its freestream state, and a downwind region in which the flow field has approximately recovered to its freestream state (Plate 1971). The dominant turbulent motions are thought to be coherent eddies produced at the windbreak top, which are analogous to the coherent motions of a spatial mixing layer (Zhuang and Wilson 1994). Although much less frequently examined, flows consisting of an array of equispaced windbreaks have also been studied (McAneney and Judd 1991; Judd et al. 1996; Patton et al. 1998; Wilson and Yee 2003). For sufficiently small spacing intervals ($\lesssim$20–30 windbreak heights; Plate 1971), the flow does not return to an equilibrium state between successive windbreaks. In this case, the mean flow field consists of standing wave-like structures with a period equal to the windbreak spacing (Wilson and Yee 2003). The structure of forest edge/clearing flows has many similar features to windbreak flows. They can be essentially considered as a very thick windbreak. At the forest-clearing interface, the flow field experiences an abrupt transition, followed by a recovery zone that extends around 20–30 canopy heights downstream. As has often been observed behind windbreaks, recirculation zones are commonly found in the wakes of a forest-to-clearing transition (Cassiani et al. 2008; Huang et al. 2011). When present, the recirculation zone is likely to have a substantial impact on scalar dispersion.

Our study seeks to examine the flow dynamics within canopies of intermediate sparseness, or canopies that lie between the relatively well-studied dense or 'closed' canopies and isolated windbreaks/shelterbelts. The objective of the study is to understand how canopy architecture interacts with the flow field to determine momentum fluxes and the general structure of turbulence in and above sparse, organized canopies. In particular, the case of a two-dimensional (2D) row-oriented canopy, characteristic of perennial crops trained using a trellis system, is explored. This is accomplished using large-eddy simulation (LES) that approximately resolves the canopy geometry. The simulations were used to provide insight into general flow behaviour of sparse canopies, as well as to determine the effect of varying row leaf area density (LAD) and row spacing on flow statistics and the structure of the turbulent flow. To understand the importance of resolving the general structure of the canopy, the results are contrasted with simulations that neglect horizontal canopy heterogeneity.

1.1 Large-Eddy Simulation of Canopy Flow

Large-eddy simulation has become a popular tool for the study of canopy-flow dynamics (Shaw and Schumann 1992; Kanda and Hino 1994; Patton et al. 1994; Su et al. 1998; Watanabe 2004; Yue et al. 2007; Dupont and Brunet 2008; Bohrer et al. 2009; Finnigan et al. 2009; Huang et al. 2009). LES solves the low-pass-filtered Navier–Stokes equations, where the filter removes turbulent motions with length scales smaller than a characteristic filter width, Δ. This method allows for control of meteorological conditions and canopy geometry, and has advantages over other approaches such as K-theory and field or wind-tunnel experiments in that it provides three-dimensional, time-resolved velocity fields with high spatial resolution.

Although LES has provided significant contributions to the understanding of turbulence structure in dense canopies (e.g., Watanabe 2004; Fitzmaurice et al. 2004; Huang et al. 2009; Finnigan et al. 2009), sparse canopies have received considerably less attention. Traditionally, LES models of canopy flow treat the canopy as continuous, horizontally homogeneous volumes of vegetation under the assumption that energetic eddies are much larger than the length scales of vegetative elements (e.g., Dwyer et al. 1997; Patton et al. 2003; Huang et al. 2009; Finnigan et al. 2009). However, as the mean spacing between vegetative elements becomes larger, the assumption of the canopy being horizontally homogeneous becomes suspect (Novak et al. 2000; Yue et al. 2007; Bohrer et al. 2009). In these canopies, the interaction between vegetative elements and open air likely has some effect on flow in the canopy, although the overall importance of these interactions is not currently well understood. It is possible that accounting for large-scale voids between vegetation may be important in capturing trends in flow statistics as the canopy becomes sparse.

In LES of canopy flow, the effects of the canopy are commonly represented by the addition of a drag term in the filtered momentum equation. This drag term arises because the direct influence of individual canopy elements (e.g., leaves, branches) is not explicitly resolved (Raupach and Shaw 1982; Finnigan and Shaw 2008). Traditionally, the drag force term is assumed to be a function of a spatially uniform drag coefficient, the local leaf area index (a function of height only), and the square of the local wind speed (Shaw and Schumann 1992). This force is then partitioned in each coordinate direction by the local wind velocity components.

Previous researchers have questioned the assumption of horizontal heterogeneity and have used various methods to improve the representation of canopy structure. Patton et al. (1995) was perhaps the first to use LES and resolve canopy heterogeneity. This study found that for a dense canopy with flow orthogonal to the row direction, various canopy representations yielded nearly identical horizontally-averaged statistics. Yue et al. (2007) performed LES of a relatively dense corn canopy where the spatial arrangement of individual plants was approximately resolved and drag from stems and leaves was accounted for independently. Their numerical representation of plant elements had an impact on horizontally-averaged statistical profiles, as well as on turbulence structure, although it is unclear whether these differences arose from resolving spatial canopy structure or from the representation of drag. Bohrer et al. (2009) also decomposed the canopy drag force into stems and leaves and reduced the volume and cell-surface area for grid cells that contained tree stems. The reduced cell surface areas and volume provided a mechanism to represent realistic flow acceleration or deceleration in the canopy trunk space. Bohrer et al. (2009) found that their canopy model produced mean turbulence statistics in good agreement with observations but they did not examine the difference between their model and a more traditional horizontally homogeneous canopy representation.

2 Numerical Simulation

The LES numerical code used in this study is described in detail in Stoll and Porté-Agel (2006a, 2008), and only a brief description of the main features is given here. The numerical treatment solves the rotational form of the low-pass filtered Navier–Stokes equations

$$\frac{\partial \tilde{u}_i}{\partial t} + \tilde{u}_i \left(\frac{\partial \tilde{u}_i}{\partial x_j} - \frac{\partial \tilde{u}_j}{\partial x_i} \right) = -\frac{\partial \tilde{p}^*}{\partial x_i} - \frac{\partial \tau_{ij}}{\partial x_j} + F_i + D_i, \tag{1}$$

where, the tilde (˜) denotes the LES filtering operation at filter width Δ, $\tilde{u}_i$ (using index notation: $1 = u$ = streamwise, $2 = v$ = spanwise, $3 = w$ = wall-normal) is the filtered velocity component in the ith direction, $x_i = x, y, z$ is the spatial coordinate in the ith direction, $\tilde{p}^* = \tilde{p} + \frac{1}{2}\tilde{u}_j\tilde{u}_j$ is the filtered dynamic pressure, F_i is a general forcing term, D_i is the drag force imposed on the flow as a result of canopy elements, and τ_{ij} is the subgrid-scale (SGS) stress tensor defined as $\tau_{ij} = \widetilde{u_i u_j} - \tilde{u}_i\tilde{u}_j$. In Eq. 1 the effects of viscous, buoyant, and Coriolis forces have been neglected. Due to the high Reynolds numbers in the canopy sublayer and the focus on near-canopy dynamics, viscous and Coriolis forces are expected to be small and are therefore assumed to be zero. Likewise, although thermal effects might play an important role in canopy momentum transport, they are neglected as they are not a focus of the study.

The SGS stress τ_{ij} must be parametrized as a function of the resolved velocity field. In this study, the SGS stress is modelled using the scale-dependent Lagrangian dynamic Smagorinsky model developed by Stoll and Porté-Agel (2006a). This model dynamically adjusts the SGS model coefficients along fluid particle trajectories making it ideally suited for LES of complex canopy flows. Previously, it has been successfully applied to other horizontally heterogeneous flows including surface roughness transitions under neutral and thermally stratified conditions (Stoll and Porté-Agel 2006a, 2009) and for flow over sinusoidal hills (Wan et al. 2007).

The domain of size $L_x \times L_y \times L_z$ is discretized onto a uniform grid of spacing Δ_x, Δ_y, Δ_z. The grid is staggered in the vertical direction and collocated in the horizontal directions. Horizontal derivatives are computed using a Fourier pseudospectral differencing scheme, a popular method for LES of both homogeneous and heterogeneous canopies (Patton et al. 1998; Yang et al. 2006a,b; Yue et al. 2007; Cassiani et al. 2008; Finnigan et al. 2009). Vertical derivatives are calculated using second-order central differences, time integration is performed using a second-order Adams–Bashforth scheme, and the non-linear terms in the code are fully de-aliased using the 3/2 rule (Canuto et al. 1988). Test filtering for the scale-dependent procedure is performed using a sharp spectral cut-off filter at scales of 2Δ and 4Δ, where $\Delta = \left(\Delta_x \Delta_y \Delta_z\right)^{1/3}$.

The lateral boundary conditions are assumed to be periodic, resulting in an infinitely repeating canopy in the horizontal directions, and the upper vertical boundary is a zero-stress rigid lid. Boundary conditions at the land surface require specification of the surface stress as a function of the local, instantaneous filtered velocity at the lowest computational level. This stress is specified by applying Monin–Obukhov similarity theory locally at every point at each timestep. Although Monin–Obukhov similarity theory is strictly only valid for homogeneous steady flows, it has been widely used in LES of the atmospheric boundary layer (ABL) due to the lack of a well-accepted alternative (e.g., Mason and Callen 1986; Albertson and Parlange 1999; Stoll and Porté-Agel 2006a,b; Yue et al. 2007). In canopy flows, the surface boundary condition is not expected to have a strong impact on flow dynamics for two reasons. First, the presence of the plant canopy results in elevated shear stress far in excess of the surface

shear stress (see, for example, Shaw and Schumann 1992, or Fig. 5) and second, Stoll and Porté-Agel (2006b) found that the effects of the surface boundary condition on flow dynamics are confined to the lowest few grid levels.

The effects of the canopy have been represented by the addition of a canopy drag term in the momentum equation, which arises due to the fact that the effects of individual canopy elements have not been explicitly resolved (Raupach and Shaw 1982; Finnigan and Shaw 2008). The focus of this study is on the impact of canopy architecture on flow dynamics and not on the development of new LES canopy-drag models. Therefore, a well-established drag model that can be easily manipulated for this purpose has been chosen over some of the more recently suggested approaches (e.g., Shaw and Patton 2003; Chester et al. 2007; Yue et al. 2007; Bohrer et al. 2009). The drag force is calculated as

$$D_i = c_\mathrm{d}\, a\, \tilde{u_i}\, \widetilde{V}, \tag{2}$$

where c_d is the drag coefficient, a is the leaf area density, and $\tilde{V}$ is the scalar wind speed. The drag force is imposed on computational nodes where canopy vegetation exists. By using a horizontal grid spacing that is on the scale of the plants, the canopy structure can be approximately resolved (see Fig. 2). For this study, flow in row-oriented canopies characteristic of grapevines grown on trellis/training systems that are oriented in parallel rows are simulated. Section 2.1 includes further details of how different canopy geometries were created.

2.1 Canopy Geometries

Here, different canopy geometries were created by manipulating the leaf area density, a, in Eq. 2. LAD is prescribed at every computational node ($LAD = 0$ where there is no vegetation). Two different canopy representations were used to determine the impact that canopy heterogeneity has on flow dynamics: a continuous representation and a discontinuous representation. The discontinuous representation specifies the LAD as homogeneous in the spanwise direction, a "square-wave" function in the streamwise direction, and a continuous function of height in the vertical direction. This effectively breaks the canopy up into parallel rows of vegetation separated in the streamwise direction by open space. The chosen *LAD* profile is based on measured values from a vertical shoot positioned (VSP) grapevine canopy reported by Gladstone and Dokoozlian (2003), and is shown in Fig. 1. The profiles were then uniformly scaled to achieve the desired leaf area index (LAI) values. The *LAI* is a vertically integrated measure of the density of a row, and is defined as

$$LAI = \int_0^h a(z)\, dz, \tag{3}$$

where h is canopy height. $LAI = 0$ at streamwise locations corresponding to spaces between rows, and some non-zero value within vegetation. Hereafter, for the discontinuous canopy, given *LAI* values refer only to the value corresponding to streamwise locations within vegetation, which is uniform in any given row.

To illustrate the effect of canopy structure on momentum transport, simulations were performed in which row spacing and row *LAI* were varied. A total of four row spacings with values of 1.0, 2.0, 3.0, and 6.0 m were simulated. For each row spacing, a simulation was run for $LAI = 1.0$ and 3.0. With the exception of the 6-m row spacing, these values represent a wide range of overall canopy densities that are observed in actual grapevine canopies (see Johnson et al. 2003). The cases with 6-m row spacings were chosen to illustrate the characteristics of a very sparse canopy. Canopy height and row width were fixed for all

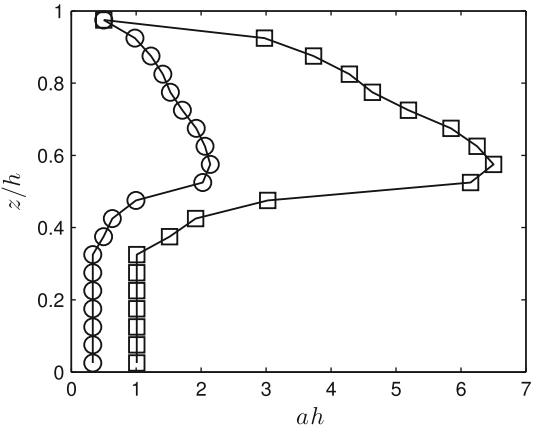

Fig. 1 Leaf area density profile of individual rows of a grapevine crop on a vertical shoot positioned trellis/training system. Symbols (*open square*) and (*open circle*) represent row $LAI = 1.0$ and 3.0, respectively

simulations, and were chosen to be 2.0 and 0.5 m, respectively. A constant drag coefficient value of 0.5 was chosen for all simulations. When a constant value of c_d is chosen, the precise value of c_d is unimportant since, in the context of the type of drag model used in this study, c_d acts to uniformly scale the *LAD* profile. Thus, this value only affects the apparent density of the canopy that can be quantified by $c_\mathrm{d}\, LAI$. The chosen value of $c_\mathrm{d} = 0.5$ is consistent with values found in the literature (e.g., Thom 1968; Cescatti and Marcolla 2004), and results in physically reasonable $c_\mathrm{d} LAI$ values. The authors also note that, in real canopies, c_d varies with position as well as wind speed, among other potential factors (Cescatti and Marcolla 2004) and that the product $c_\mathrm{d}\, a$ should have a stochastic distribution (Finnigan and Shaw 2008). In this study, c_d has been assumed constant and the product $c_\mathrm{d}\ a$ has been assumed to have a smooth distribution to keep the focus on row-scale heterogeneity.

To directly assess the impacts of canopy heterogeneity on the flow, "equivalent" horizontally homogeneous canopy simulations were performed for each of the discontinuous geometries presented above. The *LAD* profile shown in Fig. 1 was used in the continuous canopy representations, however it was scaled to have an effective *LAI* equivalent to the corresponding row-resolved simulations. The effective *LAI* can be interpreted as an average *LAI* for the entire discontinuous canopy and is defined as

$$\overline{LAI} = LAI\left(\frac{\mathcal{V}_\mathrm{r}}{\mathcal{V}_\mathrm{t}}\right) = LAI\left(\frac{r_\mathrm{w}}{r_\mathrm{w} + r_\mathrm{s}}\right), \tag{4}$$

where r_w and r_s are row width and spacing, respectively. The ratio $\mathcal{V}_\mathrm{r}/\mathcal{V}_\mathrm{t}$ is the overall volume occupied by vegetation ($\mathcal{V}_\mathrm{r}$) per unit volume of canopy ($\mathcal{V}_\mathrm{t}$). Table 1 gives the effective *LAI* values for each chosen canopy geometry.

Simulations are named according to the following convention: [R/H] $LAI \cdot r_\mathrm{s}$, where R indicates row-resolved cases and H indicates horizontally homogeneous cases. For example, the densest row-resolved simulation where $LAI = 3$ and $r_\mathrm{s} = 1$ m is named R3.1. Simulation names for all cases are given in Table 1.

2.2 Simulation Details

Simulation input parameters are given in Table 2. In all the simulations, the flow is driven by a spatially and temporally constant pressure gradient in the streamwise direction. The simulations were initialized with an approximate mean streamwise velocity profile (exponentially

Table 1 Vineyard geometry cases and their respective labels, effective leaf area indices, and line markers

LAI	r_s (m)	Case	$\overline{LAI}$	Case	Marker
3.0	1.0	R3.1	1.000	H3.1	
3.0	2.0	R3.2	0.600	H3.2	
3.0	3.0	R3.3	0.429	H3.3	
3.0	6.0	R3.6	0.230	H3.6	
1.0	1.0	R1.1	0.333	H1.1	
1.0	2.0	R1.2	0.200	H1.2	
1.0	3.0	R1.3	0.143	H1.3	
1.0	6.0	R1.6	0.077	H1.6	

Table 2 LES input parameters

$N_x \times N_y \times N_z$	$L_x \times L_y \times L_z$ (m^3)	h (m)	r_w (m)	c_d	z_o (m)	F_x (m s^{-2})
$192 \times 192 \times 160$	$48 \times 48 \times 16$	2.0	0.5	0.5	5×10^{-3}	0.025

$N_x \times N_y \times N_z$ is the number of grid points, $L_x \times L_y \times L_z$ is the domain size, h is the canopy height, r_w is the row width, c_d is the canopy drag coefficient, z_o is the aerodynamic roughness length, and F_x is the streamwise pressure gradient

decaying profile in the canopy matched to a logarithmic profile above). The initial velocity fields were given random noise with variance on the order of u_*^2. The simulations required approximately 10 eddy turnover times ($t_s\, u_*\, L_z^{-1} \approx 10$) to reach a quasi-steady state, which was defined as the time for the integral of the turbulent momentum flux profile to become constant. The simulations were performed for approximately 75 eddy turnover times at quasi-steady state ($T\, u_*\, L_z^{-1} \approx 75$), which equaled about 30 min of physical simulation time.

To maximize the domain size, it is desirable to use the minimum number of points to define the rows. Patton et al. (1998) used a single point to represent a windbreak (i.e., a single row), a choice that provides the maximum horizontal domain size for a given number of horizontal grid points. In studies using Reynolds-averaged Navier–Stokes (RANS) techniques, it is also common to represent a windbreak by a single point or Dirac-delta function (e.g., Wilson 1985). Yue et al. (2007) used three points to define the width of a plant, a choice likely dominated by the desire to resolve plant stems independently of leafy regions. To assess the minimum number of points required to resolve row structure and the general grid dependence of simulation results, three simulations were performed that used 1, 2, or 3 points to define the width of a row for a single geometry (case R3.3). Results (not shown) indicated that there were noticeable differences between the one- and two-point row representations (specifically in terms of higher-order velocity moments and dispersive fluxes) and minimal differences between the two- and three-point row representations. Thus, the present LES uses two grid points to define a row due the observation that further grid refinement has little influence on results. A schematic of the chosen numerical grid layout for the row-resolved cases is given in Fig. 2.

Ideally in large-eddy simulation of the ABL, the computational domain should be large enough to capture the full range of eddies that significantly contribute to turbulent fluxes. This requires a vertical domain height greater than or equal to the boundary-layer height and a horizontal extent greater than the boundary-layer height. The vertical and horizontal

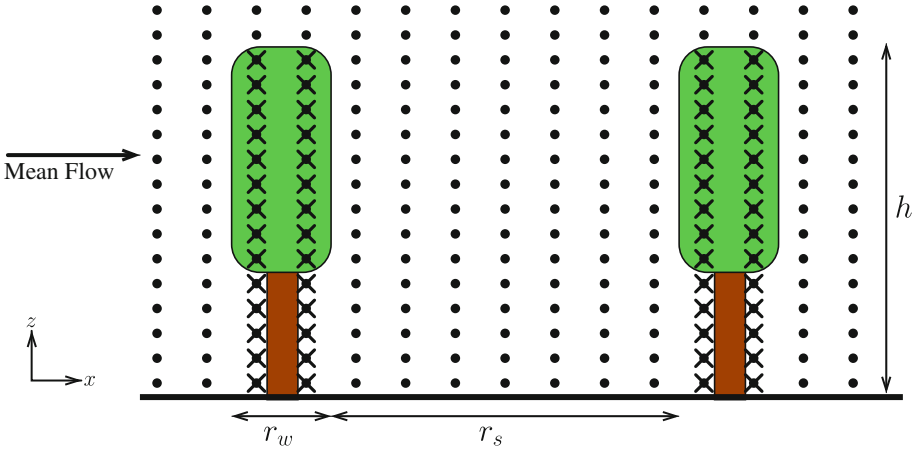

Fig. 2 Numerical representation of the simulated canopy (row-resolved). Rows repeat infinitely in the direction of the mean flow and extend continuously in the horizontal direction perpendicular to the mean flow. Symbol (*filled circle*) represents computational nodes, and (×) represents nodes at which non-zero LAD is imposed

resolutions required to resolve the canopy make this difficult. Many LESs of canopy flows have used $L_z \approx 3h$ and $L_x \approx 3L_z$ (e.g., Shaw and Schumann 1992; Kanda and Hino 1994; Patton et al. 1995; Dwyer et al. 1997; Yue et al. 2007). It should be noted that since ABL canopy flows are generally treated as inviscid, the physical height of the domain is unimportant and instead the ratio of h to L_z controls turbulent flow dynamics. For example, although the domain height of Shaw and Schumann (1992) was over five times larger than that of Yue et al. (2007), the flows are dynamically similar since the ratios of h to L_z were approximately the same. A cornerstone assumption inherent in a truncated domain height is that outer-layer structures have little influence on structures within the roughness sublayer (or the 'attached eddy hypothesis'; Townsend 1976).

In this study, the domain height was chosen to lie well below the boundary-layer height but still "sufficiently" larger than the canopy height. The present study uses a grid of $N_x \times N_y \times N_z = 192 \times 192 \times 160$ to discretize a domain of size $L_x \times L_y \times L_z = 24h \times 24h \times 8h$. To assess whether the chosen domain size was large enough, each simulation was performed using half the number of grid points in each direction with a domain that was half the size in each direction ($L_x \times L_y \times L_z = 12h \times 12h \times 4h$). Additionally, a single simulation was performed (case R3.3) that used twice the number of grid points in each direction and was twice the length in each direction ($L_x \times L_y \times L_z = 48h \times 48h \times 16h$). Results indicated that the same conclusions could be made from any of the domain size choices (results from the largest domain are shown in select figures where relevant). The range of domain sizes tested represents an increase in the dynamic range of nearly an order of magnitude. Since results hold over this range, we feel that results are relatively robust to domain size.

3 Numerical Results

3.1 Notation and Averaging

It is necessary at this point to define how statistics are formed from LES fields. We define the time averaging operator as

$$\overline{\phi_i} = \frac{1}{T} \int_{t=0}^{t=T} \phi_i(t')\, dt', \tag{5}$$

For time-averaged statistics presented in the following sections, $t = 0$ is the time at which the simulated flow field reaches a quasi-steady state and T is the total quasi-steady simulation time. The horizontal averaging operator is formally defined as

$$\langle \phi_i \rangle = \frac{1}{A} \iint_{\mathrm{R}} \phi_i \, dx \, dy, \tag{6}$$

where R is a region in the x–y plane that is large enough to remove spatial variations due to plant structure, and A is the area of region R (here, $A = L_x \times L_y$). A departure from the horizontal average is denoted by a single prime, and is defined as

$$\phi_i' = \phi_i - \langle \phi_i \rangle. \tag{7}$$

In keeping notation consistent with numerous previous numerical and experimental studies (e.g., Raupach and Shaw 1982; Poggi and Katul 2008; Calaf et al. 2010), a departure from the horizontal average of a temporally-averaged field is denoted by a double prime, and is defined as

$$\overline{\phi}_i'' = \overline{\phi}_i - \langle \overline{\phi}_i \rangle. \tag{8}$$

We define the following stress tensor (sum of turbulent and dispersive stresses and neglecting viscous stress) as

$$T_{ij} = \underbrace{\left[\overline{\langle \tilde{u}_i' \tilde{u}_j' \rangle} + \overline{\langle \tau_{ij} \rangle} \right]}_{\mathrm{I}} + \underbrace{\langle \overline{u}_i'' \overline{u}_j'' \rangle}_{\mathrm{II}}, \tag{9}$$

where term I is the total turbulent component of the stress (sum of resolved and SGS components) and term II is the dispersive component of the stress. Note that the SGS contribution to the dispersive stress is zero due to temporal averaging (i.e., $\overline{u_i - \tilde{u}_i} = 0$). The dispersive stress is identically zero in the case of a truly horizontally homogeneous flow, and can be non-zero in flows that contain regions where spatial means differ from local temporal means (Raupach and Shaw 1982; Finnigan and Shaw 2008). The concept of dispersive stresses will be further introduced and explored in Sect. 3.3.

3.2 Velocity Moment Profiles

To examine the effects of canopy geometry on mean velocity moments, vertical profiles of horizontally- and temporally-averaged velocity statistics are presented in this section. Vertical profiles are normalized either by the mean wind speed at the canopy top (U_h), or by the canopy friction velocity ($u_* = \max(|\overline{\langle \tilde{u}' \tilde{w}' \rangle} + \overline{\langle \tau_{13} \rangle}|)^{1/2}$). Values of U_h and u_* are tabulated in Table 3. Figure 3 shows profiles for wind speed, vertical momentum flux, resolved velocity variance, and resolved velocity skewness for the row-resolved canopies. For clarity, only results from representative cases are shown, where cases not shown follow the same trends. For comparison, Fig. 4 gives these same statistics for the horizontally homogeneous canopies. Figures 3 and 4 are presented for the purpose of depicting trends in velocity moments as canopy geometry is varied, with different canopy representations presented separately for clarity. Figure 5 shows a comparison of velocity moment profiles for three cases, with both canopy representations plotted on the same axes. The three cases correspond to the densest

Table 3 Bulk scaling parameters for each horizontally homogeneous and row-resolved canopy geometry

Row-resolved						Homogeneous				
LAI	r_s (m)	Case	U_h (ms^{-1})	u_* (ms^{-1})	d (m)	$\overline{LAI}$	Case	U_h (ms^{-1})	u_* (ms^{-1})	d (m)
3.0	1.0	R3.1	1.80	0.592	1.58	1.000	H3.1	1.73	0.592	1.60
3.0	2.0	R3.2	2.00	0.595	1.48	0.600	H3.2	1.81	0.591	1.54
3.0	3.0	R3.3	2.13	0.592	1.42	0.429	H3.3	2.06	0.591	1.45
1.0	1.0	R1.1	2.19	0.595	1.42	0.333	H1.1	2.21	0.592	1.41
3.0	6.0	R3.6	2.60	0.591	1.27	0.230	H3.6	2.46	0.588	1.35
1.0	2.0	R1.2	2.57	0.591	1.33	0.200	H1.2	2.59	0.592	1.33
1.0	3.0	R1.3	2.86	0.591	1.29	0.143	H1.3	2.90	0.591	1.28
1.0	6.0	R1.6	3.70	0.591	1.17	0.077	H1.6	3.63	0.591	1.18

The friction velocity is computed as $u_* = \max(|\overline{\langle\tilde{u}'\tilde{w}'\rangle} + \overline{\langle\tau_{13}\rangle}|)^{1/2}$, and the displacement height (d) is computed by the centre-of-pressure method (Thom 1971; Jackson 1981)

canopy, the canopy with largest row *LAI* and spacing, and the canopy with the lowest row *LAI* and highest row spacing (i.e., the sparsest canopy).

3.2.1 Wind Speed

The mean wind-speed profiles presented in Fig. 3a demonstrate that the strength of the inflection in the velocity magnitude profile at $z = h$ is directly related to overall canopy density. Larger canopy densities result in a stronger instability at the canopy top. Even for the lowest canopy density, there is still a clear inflection at $z = h$. The trends in the inflection at the canopy top agree with past experimental and numerical results (e.g., Poggi et al. 2004a; Huang et al. 2009). A relatively strong secondary velocity maximum is also observed in the lower canopy, which is likely due to the low-drag understorey (Shaw 1977).

Figure 5a shows that resolving row structure has little (if any) effect on the mean streamwise velocity for all geometries considered in this study. An analogous observation was also made in the LES study of Patton et al. (1994), who studied a set of infinitely repeating windbreaks oriented perpendicular to the mean flow. This result would suggest that the mean flow is dominated by overall canopy density, and not on the specifics of canopy heterogeneity. This follows naturally when considering the way in which drag is represented. Since the drag term added to Eq. 1 arises from filtering out local heterogeneity over a volume, it follows that using a filtered *LAI* (i.e., the effective *LAI*) should recover mean dynamics. Although this is the case for perpendicular flow, the study of Yue et al. (2007) indicates that this may not to be true in the case of rows oriented parallel to the mean flow, although one cannot be certain that this is due to resolving the row structure and not their drag model. Additionally, domain size appears to have a minimal effect on the mean streamwise velocity.

3.2.2 Turbulent Momentum Flux

Figure 3b shows the normalized total turbulent flux (resolved plus subgrid) for each of the row-resolved simulation cases. Above the canopy, the normalized turbulent momentum flux profile is not influenced by changes in effective *LAI*. In this region, the momentum flux linearly decreases from its maximum value located near the canopy height to a value of zero

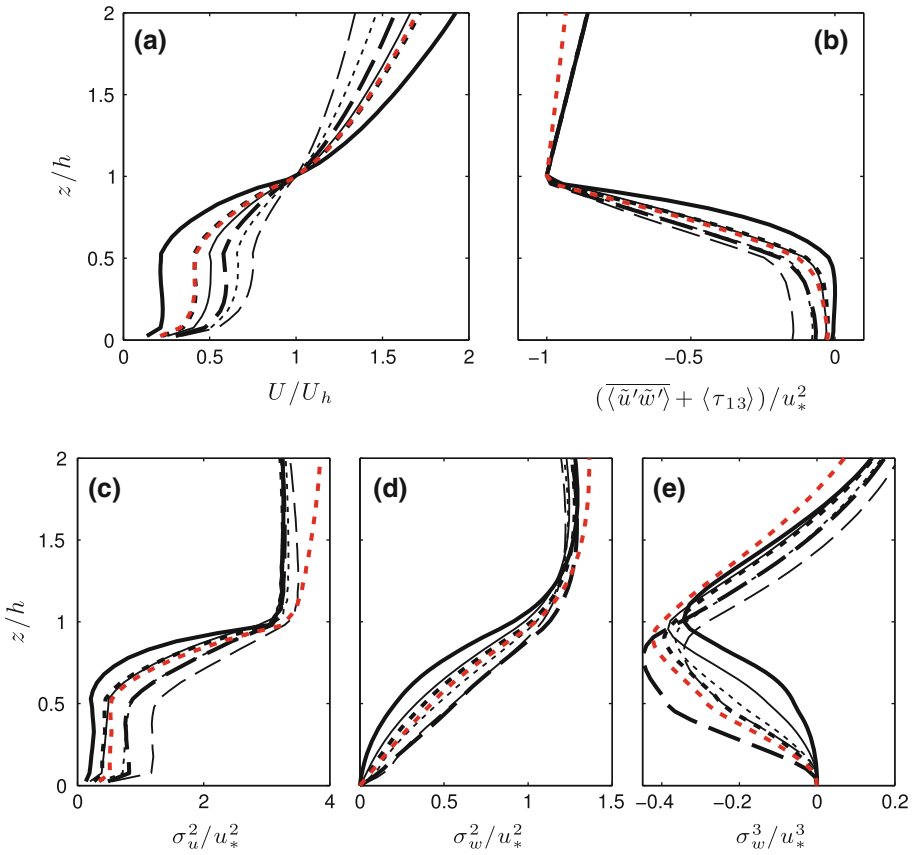

Fig. 3 Row-resolved canopy representation: comparison of velocity moment profiles for representative canopy geometries. **a** Wind speed; **b** turbulent momentum flux (sum of resolved and SGS components); **c** resolved streamwise velocity variance $\sigma_u^2 = \overline{\langle(\tilde{u}')^2\rangle}$; **d** resolved vertical velocity variance $\sigma_w^2 = \overline{\langle(\tilde{w}')^2\rangle}$; **e** resolved vertical velocity skewness $\sigma_w^3 = \overline{\langle(\tilde{w}')^3\rangle}$. R3.1 (*thick solid line*); R3.3 (*thick dotted line*); R3.3 ($384\times384\times320$) (*red thick dotted line*); R3.6 (*thick dashed line*); R1.1 (*thin solid line*); R1.3 (*thin dotted line*); R1.6 (*thin dashed line*)

at the domain height. As a result, the normalized momentum flux profile above the canopy is uniquely determined by the ratio of the domain height to the canopy height (L_z/h).

Within the canopy, the turbulent momentum flux is highly influenced by canopy density. In the canopy, the momentum flux becomes increasingly negative with decreases in effective *LAI*. This agrees with previously reported results (Poggi et al. 2004a; Dupont and Brunet 2008; Huang et al. 2009) and supports the conclusion that increased canopy density tends to suppress turbulent stress through increased drag. Furthermore, in the two densest geometries (R3.1 and R3.2) the stress at the ground is essentially zero, meaning that all mean stress has been removed by the canopy before reaching the ground.

The horizontally homogeneous canopy representation predicted a smaller momentum flux than the row-resolved representation (see Fig. 5b). For small row *LAI* or spacing, this difference was minimal, but was exaggerated as row *LAI* and spacing were increased. The largest differences occurred at the largest row *LAI* and spacing (R3.6), for which the

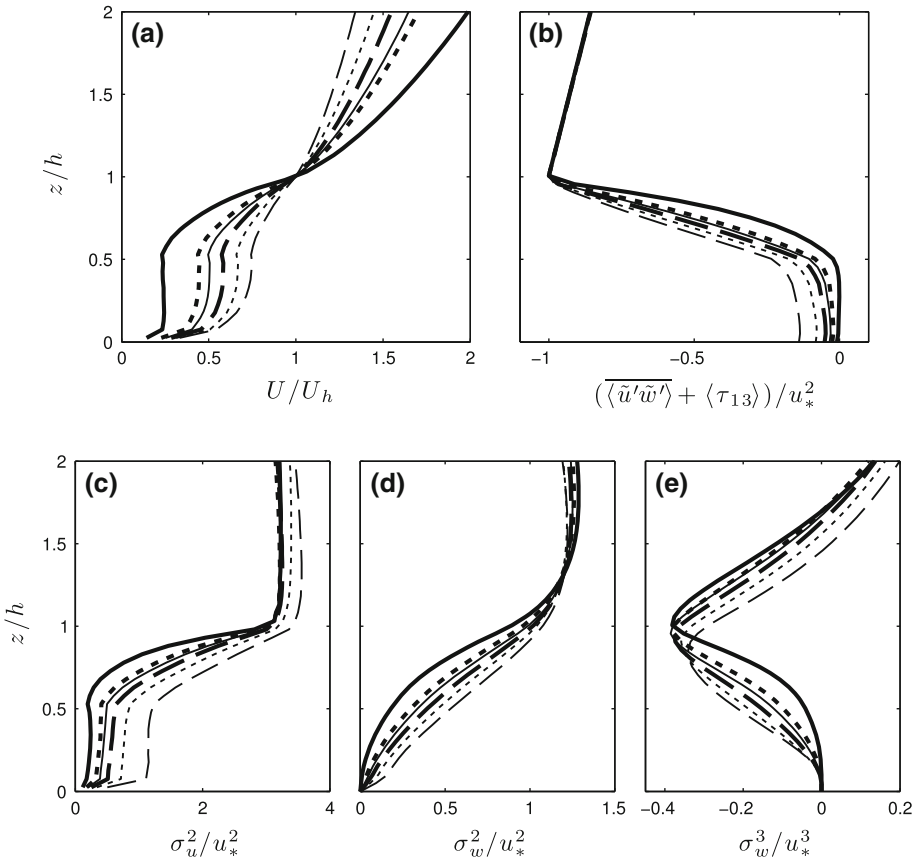

Fig. 4 Horizontally homogeneous canopy representation: comparison of velocity moment profiles for representative canopy geometries. **a** Wind speed; **b** total vertical momentum flux (sum of resolved and SGS components); **c** resolved streamwise velocity variance $\sigma_u^2 = \overline{\langle(\tilde{u}')^2\rangle}$; **d** resolved vertical velocity variance $\sigma_w^2 = \overline{\langle(\tilde{w}')^2\rangle}$; **e** resolved vertical velocity skewness $\sigma_w^3 = \overline{\langle(\tilde{w}')^3\rangle}$. H3.1 (*thick solid line*); H3.3 (*thick dotted line*); H3.6 (*thick dashed line*); H1.1 (*thin solid line*); H1.3 (*thin dotted line*); H1.6 (*thin dashed line*)

normalized momentum flux was over 50 % larger for the row-resolved canopy simulation below $z/h = 0.5$. This result can likely be attributed to the fact that, although the effective *LAI* is equivalent, the sparse canopy contains a substantial amount of open space where the flow is not directly affected by drag elements. Larger turbulent fluxes occur in these open areas, which contribute to larger horizontal averages. It is possible that the case with large row spacing but low row *LAI* (R1.6) does not show a large influence from heterogeneity due to low density canopy elements that do not significantly affect the flow field.

The within-canopy momentum flux profile trends have direct implications on the displacement height. The displacement height can be interpreted as the vertical distance the logarithmic scaling region is effectively displaced upward by the presence of the canopy. It is commonly computed by subtracting the normalized integral of the momentum flux profile ($z \leq h$) from the canopy height (Thom 1971; Jackson 1981). Since the momentum flux decreases within the canopy as canopy density is increased, the displacement height increases (see Table 3). Furthermore, since the horizontally homogeneous canopy representation

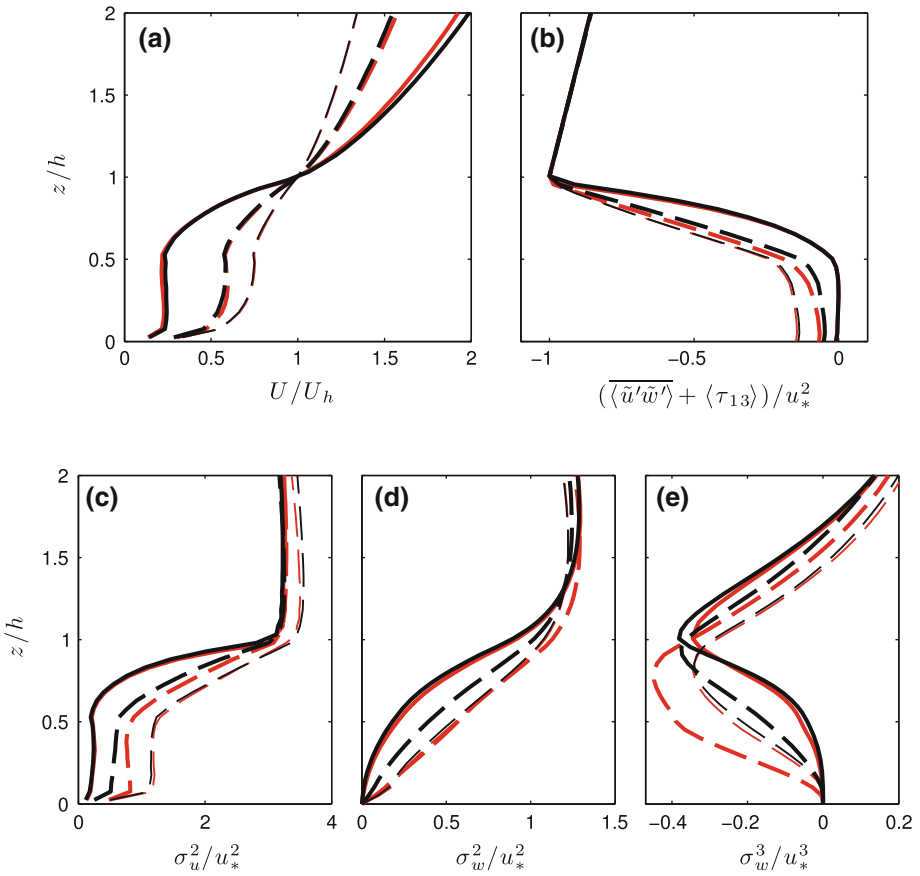

Fig. 5 Comparison between the row-resolved (*red lines*) and horizontally homogeneous (*black lines*) canopy representations for two canopy geometries. **a** Wind speed; **b** total vertical momentum flux (sum of resolved and SGS components); **c** resolved streamwise velocity variance $\sigma_u^2 = \overline{\langle(\tilde{u}')^2\rangle}$; **d** resolved vertical velocity variance $\sigma_w^2 = \overline{\langle(\tilde{w}')^2\rangle}$; **e** resolved vertical velocity skewness $\sigma_w^3 = \overline{\langle(\tilde{w}')^3\rangle}$. R3.1 (*thick solid line*); R3.6 (*thick dashed line*); R1.6 (*thin dashed line*); H3.1 (*thick solid line*); H3.6 (*thick dashed line*); H1.6 (*thin dashed line*)

underpredicts the momentum flux in cases of large row *LAI* and spacing, the displacement height is correspondingly over-predicted. However, these differences were less than 6 %, which suggests that in an integral sense the profiles in Fig. 5b show good agreement although local differences can be significant.

3.2.3 Variance

As the effective *LAI* is increased, resolved variance in the streamwise velocity component tends to be damped in the canopy. This damping of the streamwise velocity variance corresponds to the decrease in wind speed and smaller momentum flux previously discussed. A similar observation can be made regarding the vertical velocity variance.

For the horizontally homogeneous canopy, it is expected that statistics at any given height should be a monotonically increasing/decreasing function of canopy density. This

is confirmed by Fig. 4 and previous studies (Poggi et al. 2004a; Huang et al. 2009). However, for a heteogeneous canopy this is not necessarily true, as illustrated clearly by Fig. 3d. The vertical velocity variance profiles within the canopies of R3.6 and R1.6 are nearly identical even though their overall density is highly dissimilar. Several cases are out of the expected order, as profiles do not change smoothly when canopy density is varied. This indicates a high level of influence by heterogeneity on the vertical velocity variance, particularly within the canopy. This can also be seen in Fig. 5d, as there is high sensitivity to canopy representation for large row *LAI* and spacing.

The domain height has some impact on the velocity variance profiles. The effect is most evident above the canopy where a clear increase in streamwise and vertical velocity variances is observed in Fig. 5. An increase in domain height appears to allow for higher turbulence levels above the canopy. This is likely due to decreased effects of the "no-stress" upper boundary condition near the canopy.

3.2.4 Skewness

The vertical velocity skewness in the lower canopy tends to decrease as overall canopy density is increased, while the peak in the profile is effectively displaced upwards. The large negative vertical velocity skewness characteristic of canopy flows is commonly attributed to the dominance of "sweep" events, or high momentum fluid moving downward in the canopy. Thus one interpretation for the decreased skewness in the lower canopy when canopy density is increased is that turbulence structures produced near the canopy top do not penetrate into the canopy as easily in a dense canopy, and their effect is localized to near the canopy top. This is supported by decreased stress levels in the lower canopy in the dense canopy cases (see Fig. 3b).

Canopy heterogeneity has the greatest impact on vertical velocity skewness. Every geometry showed a noticeable sensitivity to canopy representation. As with previously discussed profiles, the largest differences between the homogeneous and row-resolved canopy representations were seen between R3.6 and H3.6. Figure 5d, e suggest that vertical velocity statistics are greatly affected by the presence of canopy heterogeneity in the form of increased turbulence levels and skewness. As a result, canopy heterogeneity is also likely to have an effect on the vertical mass and scalar transport.

Domain height has an effect on vertical velocity skewness. Similar to the velocity variance, the impact of domain height is largest above the canopy. Positive skewness is lower above the canopy when the domain height is increased, which indicates the effect of the canopy on the ratio of sweeps to ejections propagates upward further in the larger domain simulations.

3.3 Dispersive Fluxes

For homogeneous canopies, it is often convenient to apply the horizontal averaging operator to flow variables (e.g., Sect. 3.2). This effectively eliminates spatial variability in the horizontal direction, particularly heterogeneity at the plant scale. While horizontally averaging the conservation equations reduces the problem from three-dimensions to one and focuses modelling efforts on vertical transport, the non-commutativity of the horizontal average results in an additional stress term similar to the Reynolds stress, commonly referred to as the dispersive stress (Raupach and Shaw 1982). Physically, the dispersive stresses arise from areas of the flow where local temporal means differ from spatial means.

Often, the dispersive component of the stress is neglected. The presumption is usually made that the dispersive stress is small compared to the turbulent stress. Frequently, this

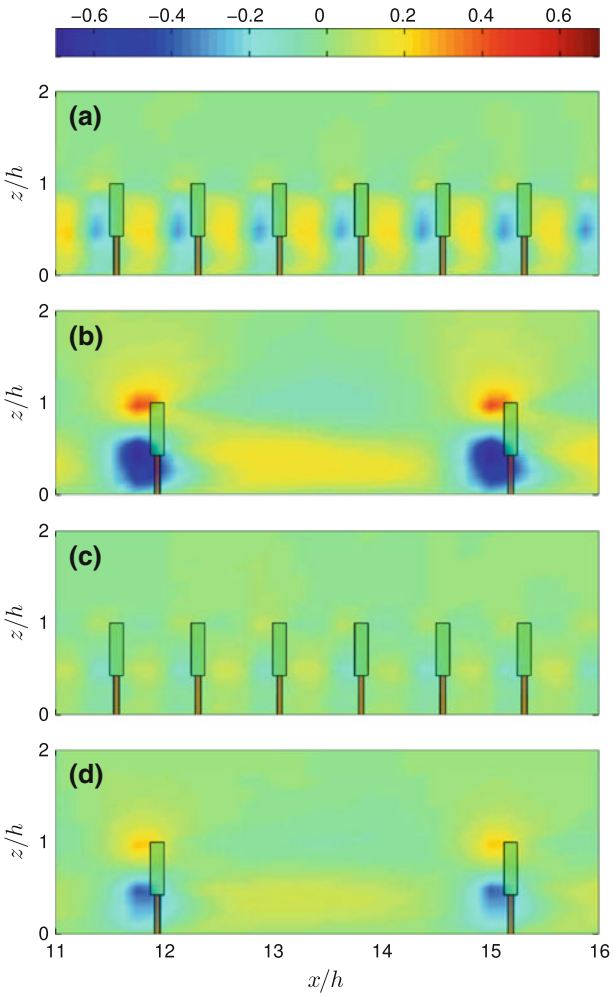

Fig. 6 Temporally- and spanwise-averaged w velocity component normalized by $\sigma_w = \overline{\langle(\tilde{w}')^2\rangle}^{1/2}$. Results are shown for a representative area extracted from the middle of the domain. **a** R3.1; **b** R3.6; **c** R1.1; **d** R1.6

assumption is made out of convenience, since the dispersive stress is difficult to measure experimentally due to the requirement of a large spatial array of sensors. However, prior studies have indicated that this assumption may be poor inside certain heterogeneous canopies (Böhm et al. 2000; Finnigan 2000; Christen and Vogt 2004; Poggi and Katul 2008).

In heterogeneous canopies, significant dispersive fluxes may arise as a result of plant-scale heterogeneity. This can have a strong influence on the mean velocity field, particularly the vertical velocity. Figure 6 depicts the normalized vertical velocity in the $x - z$ plane temporally-averaged and then spatially-averaged in the spanwise direction. A central streamwise segment is shown for representative canopy geometries. The presence of the rows acts to partially divert flow around regions of dense vegetation. Flow in the upper half of the vegetated region of the canopy is generally diverted upward, while flow in the lower half is generally diverted downward into the canopy understorey as it impinges upon a row. This

has the effect of modifying average streamlines in the canopy, which are sinusoidal with period equal to the period of the rows (i.e., $r_w + r_s$). This result generally agrees with the forest-clearing LES of Cassiani et al. (2008) and Huang et al. (2011) who both found large positive vertical velocity perturbations around $z = h$ near a clearing-to-forest transition, and large negative velocity perturbations in the wake of a forest-to-clearing transition. However, these studies do not report significant negative w perturbations in the lower canopy near the clearing-to-forest interface, even in the presence of a low-density understorey. This suggests that the small width of connected vegetation allows for significant downward transport of mass and momentum into the canopy understorey.

For the smallest row spacing, the perturbations in mean vertical velocity over horizontal plane-averaged values were very weak. For the largest row spacing, these perturbations became nearly as large as the standard deviation of the vertical velocity, σ_w. The magnitude of the mean vertical velocity in the canopy is also strongly linked to the row *LAI*. Larger *LAI* leads to larger perturbations in mean vertical velocity from horizontally averaged values, a feature also observed by Cassiani et al. (2008). When correlated with mean perturbations in the u velocity component, these local perturbations in mean w velocity contribute to dispersive fluxes.

3.3.1 A Note on Streamwise Vortices

In past wind-tunnel and numerical studies of boundary-layer flows with large roughness elements, researchers have acknowledged the presence of persistent streamwise vortices corresponding to mean spanwise heterogeneity (Brunet et al. 1994; Reynolds et al. 2007; Finnigan et al. 2009). Brunet et al. (1994) noted that, despite inflow conditioning in a wind tunnel, these structures could not be eliminated. In the LES study performed by Finnigan et al. (2009), the authors note that increasing horizontal domain size and simulation duration failed to remove this heterogeneity. These so-called streamwise vortices cause variations in spanwise transects of $\overline{u}$ that are approximately sinusoidal with a period of L_z. We also found that local maxima/minima in $\overline{u}$ corresponded to local minima/maxima in $\overline{w}$, thus they are negatively correlated. Therefore, even the simulated horizontally homogeneous canopy can generate dispersive fluxes. As a result, calculating dispersive fluxes from wind-tunnel and LES data presents a convoluted picture, since spanwise-heterogeneity-induced dispersive flux structures are superposed onto geometry-induced dispersive flux structures.

It is important to determine the influence of streamwise vortices on dispersive fluxes. One may mistakenly attribute large dispersive fluxes to canopy heterogeneity when in fact they may be due to spanwise heterogeneity that is present even in the absence of canopy heterogeneity. Spanwise heterogeneity in $\overline{w}$ is small in the lower canopy, and much larger above the canopy. This suggests that dispersive fluxes in the lower canopy are not associated with spanwise heterogeneity. In the following section, further assessment is made as to the importance of mean spanwise heterogeneity on dispersive fluxes.

3.3.2 Dispersive Flux Profiles

To directly examine the impact of the sinusoidal patterns observed in Fig. 6 on dispersive fluxes, normalized dispersive flux profiles are plotted in Fig. 7a for all of the simulated cases. The maximum dispersive flux occurs at $z/h \approx 0.4$ and increases as both row *LAI* and spacing are increased. The trends in the dispersive flux directly relate to the previously observed patterns in mean vertical velocity. The higher drag that results from denser rows causes

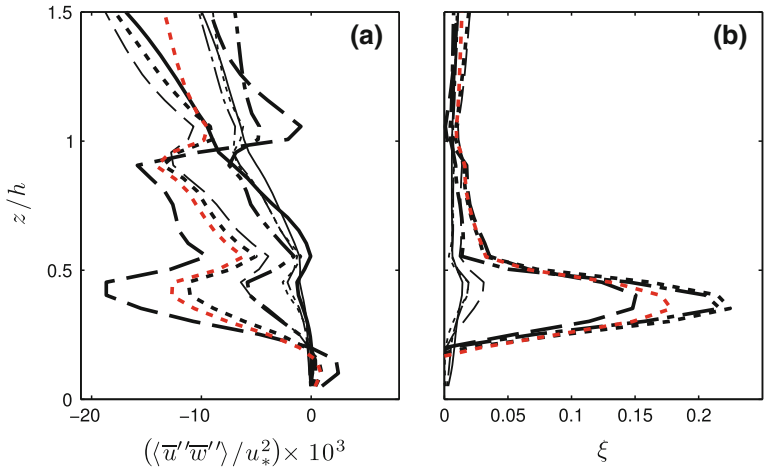

Fig. 7 **a** Normalized dispersive flux; **b** relative contribution by dispersive flux to the total vertical momentum flux. R3.1 (*thick solid line*); R3.2 (*thick dashed dotted line*); R3.3 (*thick dotted line*); R3.3 (384 × 384 × 320) (*red thick dotted line*); R3.6 (*thick dashed line*); R1.1 (*thin solid line*); R1.2 (*thin dashed dotted line*); R1.3 (*thin dotted line*); R1.6 (*thin dashed line*)

larger perturbations in mean velocity fields, resulting in larger dispersive fluxes. Although both row *LAI* and spacing influence dispersive fluxes, row *LAI* seems to be the more important factor in generating high dispersive fluxes.

An important question when examining vertical transport in sparse canopies, where voids are expected, is how important these dispersive fluxes are with respect to the total momentum flux. Following Poggi and Katul (2008), the relative importance of the dispersive flux to the turbulent flux is evaluated using the parameter

$$\xi = \frac{\langle \overline{u}''\overline{w}'' \rangle}{\langle \tilde{u}'\tilde{w}' \rangle + \overline{\langle \tau_{13} \rangle}}, \tag{10}$$

which is simply the ratio of the dispersive flux to the turbulent momentum flux (sum of resolved and SGS components). Figure 7b gives profiles of ξ. Note that the case R3.1 has been excluded from Fig. 7b, because both turbulent and dispersive stresses are very small in the lower canopy and thus ξ is not a relevant metric.

Above $z/h \approx 0.5$, dispersive fluxes are negligible for all canopy geometries due to large turbulent stresses. However, in the lower half of the canopy, dispersive fluxes can account for a significant fraction of the total vertical flux. This is similar to results reported by Poggi et al. (2004b), who found that in the lower canopy region, dispersive fluxes in a sparse canopy accounted for up to 30 % of the turbulent momentum flux, whereas dispersive fluxes were negligible for dense canopies. Böhm et al. (2000), Cheng and Castro (2002), Christen and Vogt (2004) and Poggi and Katul (2008) all made similar conclusions. We also note that in the horizontally homogeneous canopy, which contains non-zero dispersive fluxes due to spanwise heterogeneity, dispersive fluxes were negligible (< 1 %) at all heights in the domain when compared to the turbulent flux. Thus, we can conclude that the large dispersive fluxes in the lower canopy are a result of streamwise canopy heterogenity and not mean spanwise flow heterogeneity.

Although the dispersive flux increases as row spacing is increased, the relative contribution to the total flux by the dispersive flux does not necessarily follow this behaviour. The turbulent

flux increases at a faster rate than the dispersive flux as row spacing is increased. Although it may be difficult to directly interpret trends in ξ, some general conclusions can be made. For geometries in which row spacing is small or row *LAI* is small, dispersive fluxes are negligible. However, for large row *LAI* or spacing, normalized dispersive fluxes were over 20 % as large as the normalized turbulent momentum flux near mid-canopy height. Recall that the homogeneous canopy representation also underpredicted the turbulent momentum flux by up to 50 % near mid-canopy height in the case of H3.6/R3.6. This suggests that resolving large-scale voids between vegetation may be important in terms of predicting correct total momentum fluxes (sum of turbulent and dispersive components).

Since non-zero dispersive fluxes have the potential to increase the total flux (see Eq. 9), bulk parameters derived from the flux profile may also be affected. Including dispersive fluxes in friction velocity calculations ($u_*^2 = \max|T_{13}|$) had little impact, and is a result of negligible dispersive fluxes at the canopy top (see Fig. 7b). In terms of integral quantities such as the canopy displacement height, dispersive fluxes also had a negligible effect due to the fact that most of the area under the momentum flux profile is in the upper canopy where dispersive fluxes are small. Displacement heights that included dispersive fluxes resulted in a reduction in d of no more than 2 % compared to d values that only included the turbulent flux. This follows logically from the observation that mean streamwise velocity profiles show little sensitivity to canopy heterogeneity (Fig. 5a). It is also noted that since U, u_* and d are not significantly affected by canopy heterogeneity, the aerodynamic roughness length z_o should also be unaffected (Stull 1988). From this we conclude that, for the range of sparse canopy geometries studied here, assuming horizontal homogeneity results in minimal errors in these scaling parameters, which are commonly used in bulk parametrizations.

Domain height had a slight influence on dispersive fluxes. Increased domain height resulted in a small increase in dispersive fluxes within the canopy due to canopy heterogeneity. Slightly smaller ξ values are seen with increased domain height, although this is a combined effect of changes due to dispersive and turbulent fluxes.

3.4 Turbulence Structure

Identifying and understanding coherent turbulent structures in canopy flows has become a primary focus of many canopy transport studies. This is motivated by the need to explain and model the unique turbulent dynamics within the canopy layer. These dynamics include highly coherent turbulent eddies that appear to be exceptionally efficient at transporting momentum and scalars even in the presence of small gradients.

For the geometries and flow configuration considered in this study, there are two primary types of structures to consider with regards to fluxes near the canopy. The first are mixing-layer-like structures that give considerable contributions to turbulent fluxes and are thought to be generated by an inviscid instability mechanism at the canopy top (Raupach et al. 1996; Finnigan 2000; Finnigan et al. 2009). According to Finnigan et al. (2009), these structures consist of an upstream head-down hairpin vortex that generates strong sweep events paired with a downstream head-up hairpin vortex that generates weaker ejection events. The second type of structures are "standing" wavy structures that form as a result of row structure and can give considerable contributions to dispersive fluxes. These two types of structures are explored in the following sections.

As the canopy becomes very sparse and undergoes transition to a pure boundary layer, structures produced by wall shear may also become important near the canopy (Robinson 1991). The following section also presents evidence that these structures are not expected to be important near the canopy for the range of geometries considered in this study.

3.4.1 Turbulent Length Scales

Some of the most important parameters to understand in any turbulent flow are the characteristic turbulent length scales and their association with turbulent fluxes. Assuming applicability of the mixing-layer analogy, the high shear region created by the presence of the canopy creates Kelvin–Helmholtz-like coherent vortices that are advected in the streamwise direction. Λ_x is interpreted as the mean streamwise separation distance between these coherent structures (Shaw et al. 1995; Raupach et al. 1996), and is thought to be the dominant turbulent length scale in dense canopies. A commonly used method of estimating this length scale is to relate Λ_x to the integral length scale of the w velocity component at the canopy top. This is often determined from one- or two- point autocorrelation functions (among other methods, see Shaw et al. 1995). The two-point zero time-lag autocorrelation function for the vertical velocity is defined as

$$r_{ww}(x, y, z; z_R) = \frac{\overline{w(x, y, z)w(0, 0, z_R)}}{(\overline{w'^2(z)})^{1/2}(\overline{w'^2(z_R)})^{1/2}}, \tag{11}$$

where z_R is a reference height. The two-point integral length scale is found by integrating the autocorrelation function along a streamwise transect at the canopy top

$$L_w^{\cdot\cdot} = \int_0^\infty r_{ww}(x, 0, h; h)\, dx, \tag{12}$$

which is related to Λ_x by a factor of 2π (Raupach et al. 1996). By analogy with a true mixing layer, Λ_x is expected to scale linearly with the shear length scale $L_s = U_h/(dU/dz)_{z=h}$. Raupach et al. (1996) found that $\Lambda_x = 8.1L_s$ by performing a linear regression analysis on experimental data. Figure 8 plots the relationship between L_s and Λ_x calculated from the autocorrelation function for the simulated canopies as well as data obtained from the LES studies of Huang et al. (2009) and Dupont and Brunet (2008). Results are shown only for the homogeneous canopies as integral length scales showed little sensitivity to canopy representation (see Fig. 9). The studies of Novak et al. (2000), Dupont and Brunet (2008), and Huang et al. (2009) all found that above a normalized shear length of about $L_s/h = 0.6$, the linear relationship between L_s and Λ_x failed to hold and Λ_x/h asymptoted to a value near 5.0. Each study concludes that below some critical canopy density, there is not a strong enough inflection in the mean velocity profile to generate the mixing-layer structures and thus at this point the flow no longer resembles a mixing layer. The simulated canopies of the present study behave similarly to that of Novak et al. (2000); Dupont and Brunet (2008) and Huang et al. (2009), in that after some critical canopy density, Λ_x is approximately independent of L_s. The shear-independent value of Λ_x/h is approximately the same for the past studies as well as the present LES.

To assess whether the shear-independent value of Λ_x/h truly corresponds to the pure boundary-layer case, a simulation was performed with identical input parameters as the previously described canopy cases, except that $LAD = 0$ everywhere (i.e., a 'no-canopy' case). The value of Λ_x for this case is indicated by a dashed line in Fig. 8. For the sparse canopy cases, Λ_x indeed asymptotes to this rough-wall boundary-layer value. The integral length in a turbulent boundary layer scales as κz, where κ is the von Karman constant (Pope 2000). Λ_x/h should be on the order of the theoretical value $2\pi\kappa$, which is consistent with Fig. 8.

The present LES supports the conclusions of Dupont and Brunet (2008) and Huang et al. (2009) that the shear-independent behaviour of Λ_x observed in sparse canopies can be

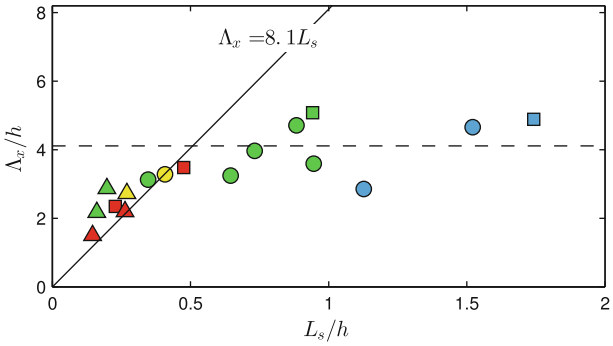

Fig. 8 Relationship between Λ_x and L_s for a wide range of canopy densities, where Λ_x is calculated from the two-point autocorrelation function r_{ww} at a reference height of $z = h$. (*circle*) Present LES; (*triangle*) Dupont and Brunet (2008) LES; (*square*) Huang et al. (2009) LES. *Red* $0.75 \leq c_d\ LAI$; *yellow* $0.5 \leq c_d\ LAI < 0.75$; *green* $0.1 \leq c_d\ LAI < 0.5$; *blue* $c_d\ LAI < 0.1$. The *horizontal dashed line* is the Λ_x / h value corresponding to the $\overline{LAI} = 0$ or "no-canopy" case

attributed to the transition from a canopy flow to a rough-wall boundary-layer flow. It is important to note that, although Fig. 8 supports this conclusion, the vertical velocity skewness profiles in Figs. 3e and 4e indicate that sweep events are dominant in even the sparsest canopy cases (i.e., negative skewness near the canopy). This inconsistency is further investigated in Sects. 3.4.3 and 3.4.4, which support the conclusion of the present study that even relatively sparse canopies can continue to behave predominantly as canopy layers.

3.4.2 Dispersive Length Scales

Length scales associated with dispersive fluxes were estimated using spectra of the vertical velocity. Figure 9 shows compensated w spectral energy density calculated in the streamwise direction and averaged in the spanwise direction for both canopy representations. Above the canopy, the energy spectrum resembles that of a turbulent boundary layer, with a classical Kolmogorov $-2/3$ isotropic scaling region observed for wavenumbers $k_x > 3h$. Within the canopy, a $-2/3$ isotropic region is not present. Vertical velocity spectra obtained from experiments have produced conflicting results. Some experimentalists have reported a $-2/3$ region (Amiro 1990), while others have reported that energy is dissipated at a lower or higher rate at small scales (Amiro 1990; Kaimal and Finnigan 1994). All the present LESs tend to dissipate energy at a higher rate than the classical Kolmogorov spectrum, an effect that becomes more pronounced as the effective *LAI* is increased.

The spectra for the row-resolved canopy representation shows significant spikes for wavenumbers of $k_x h > 1$, which are absent in the horizontally homogeneous canopy representation simulations. These spikes occur at wavenumbers corresponding to the row wavelength (i.e., $r_w + r_s$). The magnitude of these spikes decrease slightly with decrease in row spacing and, for $LAI = 3$, are the highest energy waves, indicating that $r_w + r_s$ is an important length scale. Spectral spikes were also observed in the row-resolved simulations of Yue et al. (2007), who also concluded that these spikes were a result of the periodic nature of drag elements.

Although these spectral spikes can be large in magnitude, they contain a relatively small amount of energy in an integral sense, and therefore do not significantly affect the integral length scales previously discussed. Similar to perturbations in the mean w, spikes in the

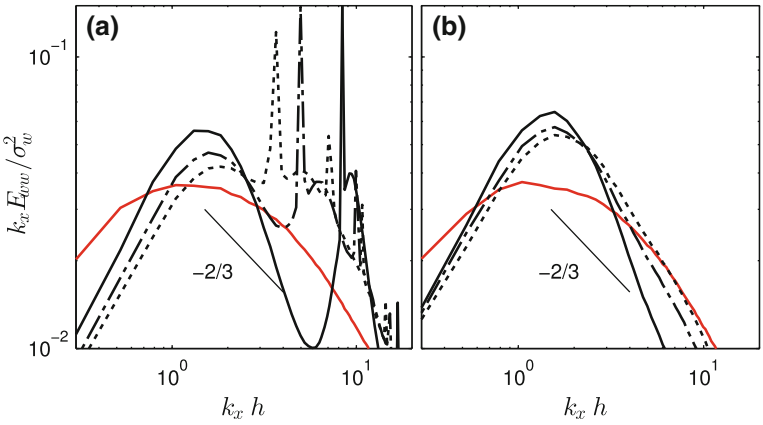

Fig. 9 Compensated w spectra for representative vineyard geometries. **a** Row-resolved canopy representation; **b** horizontally homogeneous canopy representation. R3.1 (*thick solid line*); R3.2 (*thick dashed dotted line*); R3.3 (*thick dotted line*); *black lines* $z = 0.4h$ (approximate height of maximum dispersive flux); *red lines* $z = 4h$

spectra are minimal for $LAI = 1$. Aside from the spike corresponding to the row wavelength, smaller spikes occur at the wavelengths of the sub-harmonics of the wave motions corresponding to the first spectral spike.

3.4.3 Quadrant-Hole Analysis

Although it is difficult to precisely determine the contributions of coherent structures to fluxes in canopy flows, one popular method of approximating this importance is through the use of quadrant-hole analysis (Lu and Willmarth 1973). In this method, two-dimensional velocity fluctuation vectors are grouped into quadrants; most commonly $\{u', w'\}$ vectors are considered. For example, a vector with positive components of u' and w' would be termed a "Quadrant 1" or "Q1" event because the vector points into the first quadrant. Vectors that point into Q2 (i.e., $-u'$ and $+w'$) are termed "ejection" events and vectors that point into Q4 (i.e., $+u'$ and $-w'$) are termed "sweep" events. Only vectors greater than a given magnitude $\mathcal{H}$ (termed the hole size) are considered in quadrant-hole analysis, where $\mathcal{H}$ determines the "size" of structures being analyzed.

Profiles of the relative contributions to the vertical momentum flux of Q2 events to Q4 are shown in Fig. 10. Note that here fluctuation vectors were calculated as deviations from plane averages of filtered variables (i.e., $\{\tilde{u}', \tilde{w}'\}$), and that the hole size was set to a value of $\mathcal{H} = 0$. Four representative canopy geometries are shown, as well as the $\overline{LAI} = 0$ case. In all four of the canopy cases, similar features can be observed, which are also consistent with several previous studies examining various canopy types (e.g., Baldocchi and Hutchinson 1987; Christen and Vogt 2004; Finnigan et al. 2009). In the upper half of the canopy, sweep events contribute substantially more to the flux than ejection events. Above a height of $z/h = 1.5$, ejections begin to dominate sweeps. For the densest canopies (most notably R3.1), it is observed that a region exists in the lower half of the canopy in which ejections give a larger contribution to the flux than do sweeps. This region grows vertically with an increase in overall canopy density. Profiles change slightly when the horizontally homogeneous canopy representation is used, although the same general characteristics remain consistent. This is

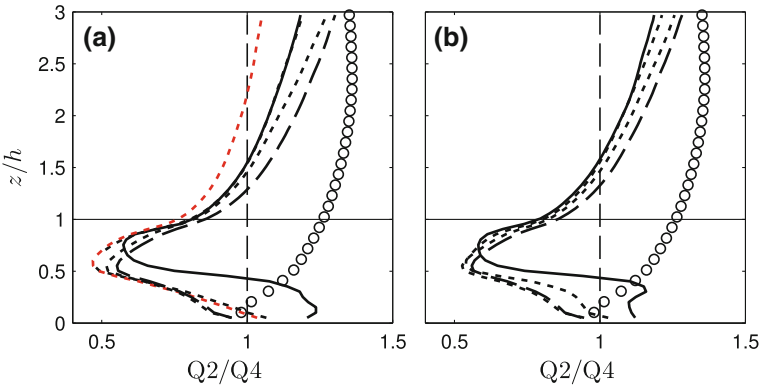

Fig. 10 Profiles of the ratio of contributions to the momentum flux by ejection events to sweep events. **a** Row-resolved canopy representation; **b** horizontally homogeneous canopy representation. R3.1 (*thick solid line*); R3.3 (*thick dotted line*); R3.3 ($384 \times 384 \times 320$) (*red thick dotted line*); R1.3 (*thin dotted line*); R1.6 (*thin dashed line*); $\overline{LAI} = 0.0$ (*open circle*)

an indication that the general structure of turbulence is not largely influenced by canopy heterogeneity.

The profile corresponding to the simulation of $\overline{LAI} = 0$ illustrates the case of a rough-wall boundary layer (equivalent to an infinitely sparse canopy). Note that for this case the vertical coordinate was also normalized by h for consistency, although this is clearly not the relevant scaling parameter. Without a canopy, ejections dominate sweeps throughout the domain. The exception to this is near the wall, where the LES surface boundary condition adversely affects resolved velocity field fluctuations (Stoll and Porté-Agel 2006b). When the profile corresponding to the "no-canopy" case is compared to the sparsest canopy geometry (R1.6), we observe that even the sparsest canopy behaves more like a canopy layer than a boundary layer in the near-canopy region. This suggests that the sweep-generating coherent structures characteristic of near-canopy flow still dominate the vertical momentum flux in the sparse canopy cases. This result is in opposition to the conclusion that can be drawn from Fig. 8, which is that based on integral length scales at the canopy top, the structure of turbulence in sparse canopies is more like that of a rough-wall boundary layer than a canopy layer. We conclude that integral length scales at the canopy top are not indicative of the presence of canopy-layer structures in sparse canopies, and that these structures still dominate turbulent fluxes as the canopy becomes sparse. Coherent turbulent structure detection will be used in the next section to further illustrate this point.

3.4.4 Characteristic Eddy Structure

Autocorrelation analysis and vertical velocity spectra have provided a means of determining the dominant length scales in sparse, organized canopies. To further investigate the impact of canopy geometry and density on the flow, the spatial structure of turbulence in the canopy is characterized in this section. In the horizontally homogeneous canopy, conditional averaging techniques have become a popular way of characterizing coherent structures that occur at random horizontal locations in the canopy (Zhou et al. 1999; Finnigan and Shaw 2000; Watanabe 2004; Finnigan et al. 2009). These techniques generally involve composite averaging independent realizations of the flow field based on a characteristic trigger event. In this section, the method of Finnigan et al. (2009) was used to give a graphical representation of

the structure of turbulence. A coherent turbulent eddy was identified by locating instantaneous positive peaks in the pressure perturbation (i.e., $\tilde{p}'$) at the top of the canopy. Regions of pressure higher than a predefined threshold pressure, $p_{\mathrm{T}} = \alpha u_*^2$, were used to define local coordinate systems in which the origins, $\{r_x, r_y\} = \{0, 0\}$, lay at the local maxima of the pressure regions. Local maxima within a specified radius of a larger maximum were neglected. Instantaneous volumes of fluctuating velocity fields (i.e., $\tilde{u_i}'$) that have local coordinates centred at the local maxima in pressure perturbation were extracted from the domain. A total of $\mathcal{M}$ volumes of size $W \times W \times L_z$ and centred at $\{r_x, r_y\} = \{0, 0\}$ were extracted from instantaneous $\tilde{u_i}'$ and $\tilde{p}'$ fields and composite averaged to obtain information about the spatial structure of a "characteristic" eddy. For further details on the detection method, consult Finnigan et al. (2009).

Figure 11 shows vectors of $\{\tilde{u}', \tilde{w}'\}$ taken from an $x - z$ slice through the centre of the composite-averaged structure for both canopy representations. This slice is representative of behaviour throughout the composite structures, and therefore other views are not shown. Four different canopy geometries representative of the range of tested densities are presented in Fig. 11. These structures show that, even for a relatively sparse canopy, nearly identical structures are seen in the dense and sparse canopies. This result, along with the results of quadrant-hole analysis, indicates that, although in the sparsest canopies the integral length scale at the canopy top is indicative of rough-wall boundary-layer behaviour, the mixing-layer-like structures are still present and appear to strongly influence vertical fluxes.

The magnitudes of sweep and ejection vectors from the characteristic eddy depicted in Fig. 11 remain relatively constant with changes in the effective *LAI*. The main change as canopy density is varied is the level of penetration of the structure into the canopy. Along with the relative elongation of the characteristic eddy shown by the fluctuation vectors, the visualization of structure penetration is aided by overlaid isocontours of composite-averaged pressure fluctuations. Conditional averaging illustrates that structures presumably generated at the canopy top penetrate further into the canopy, a feature consistent with trends in the "mixing" or shear length scale L_{s}. This result agrees with Figs. 3e and 4e, which showed that regions of large negative vertical velocity skewness are localized to near the canopy top in the denser canopy cases and extend further toward the wall in the sparser canopies. Analogously, the results of quadrant-hole analysis (Fig. 10) showed that the region in which sweep events dominated ejection events extended further toward the wall in the sparser canopy cases.

Figure 11 also indicates that structures penetrated further into the canopy in the row-resolved simulations than in the horizontally homogeneous canopy in most cases. This was most pronounced in cases of large open spaces between vegetation (i.e., large row spacing). A similar result was observed in the vertical velocity skewness profile and quadrant-hole analysis plots, where large negative skewness values and the dominance of sweeps over ejections extended deeper into the canopy in the row-resolved cases with large row spacing. This is likely due to the fact that the row-resolved canopies contain a significant fraction of open space, allowing structures to penetrate further into the canopy on average.

Although the horizontally homogeneous and row-resolved canopy representations yield very similar characteristic eddy structures, it is possible that canopy heterogeneity may have an effect on the production of structures. To investigate this, the streamwise locations of pressure trigger events were recorded. A one-dimensional "row-local" coordinate system was established in which the centre of a vegetative row is defined as the origin, $x_\ell = 0$. The position of a pressure trigger event is defined with respect to the nearest vegetative row, thus $x_\ell \in (-0.5(r_{\mathrm{w}} + r_{\mathrm{s}}), 0.5(r_{\mathrm{w}} + r_{\mathrm{s}})]$.

Figure 12 gives the row-local locations of pressure trigger events, which correspond to the pressure spikes used to form the composite structures shown in Fig. 11. For clarity,

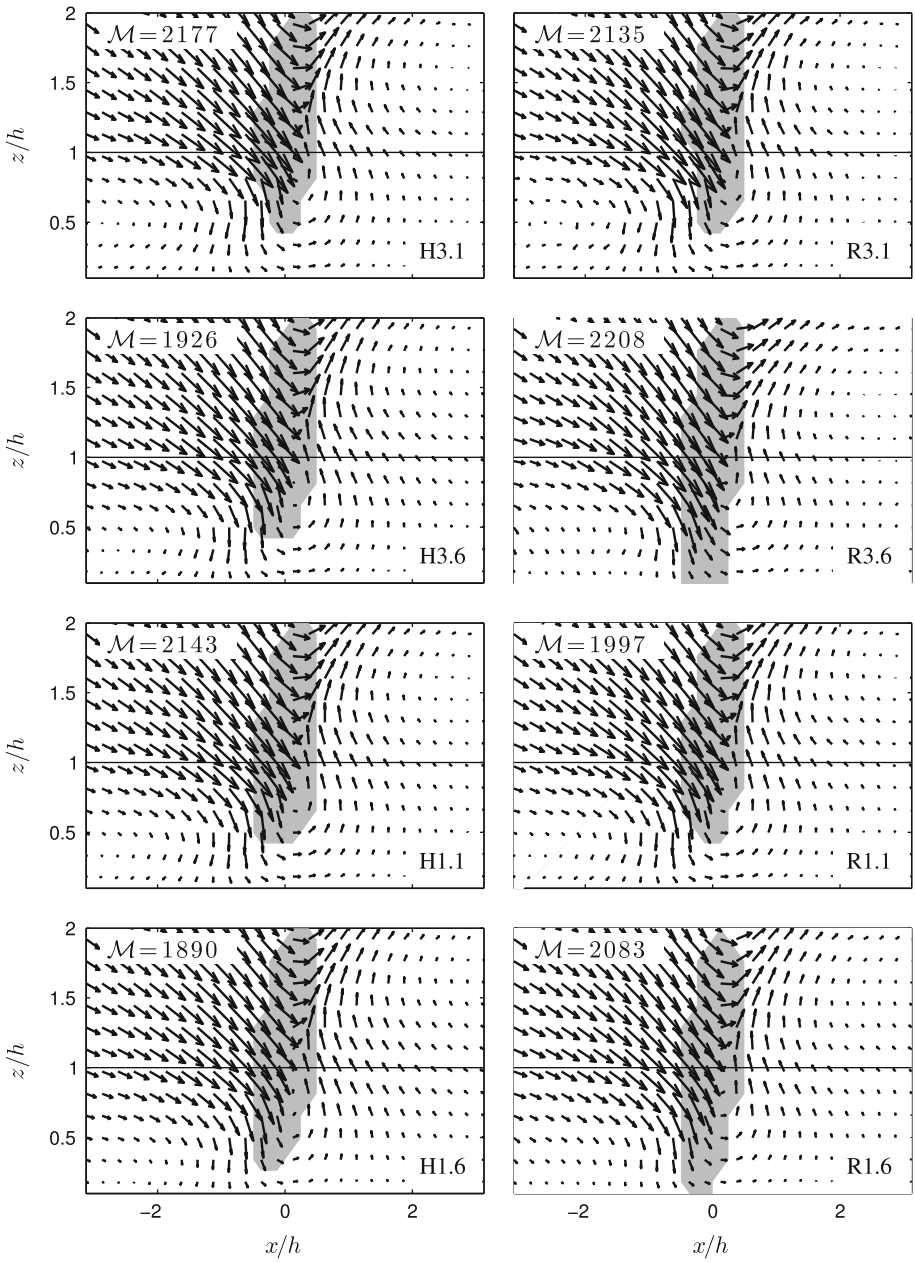

Fig. 11 Vectors of $\{\tilde{u}', \tilde{w}'\}$ corresponding to a slice in the $x - z$ plane through the centre of a composite eddy formed by conditionally averaging triggered by pressure spikes. The pressure threshold coefficient used had a value of $\alpha = 3.0$. *Shaded regions* show pressure larger than $3u_*^2 = p_T$. The *left* and *right columns* correspond to the horizontally homogeneous and row-resolved canopy representations, respectively. The number of realizations used to form each structure is given by $\mathcal{M}$

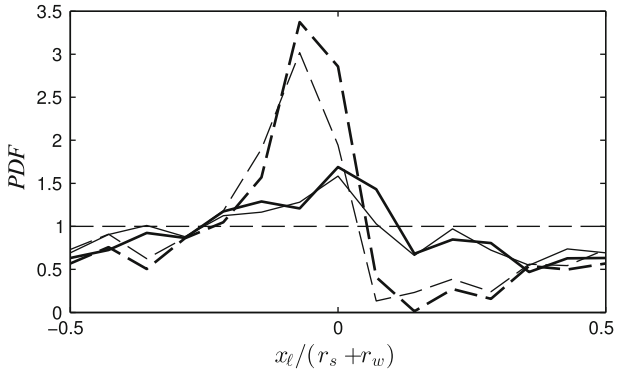

Fig. 12 Streamwise location of pressure trigger events used to identify coherent turbulence structures. Locations are given in normalized row-local coordinates, where $x_\ell/(r_\mathrm{s} + r_\mathrm{w}) = 0$ corresponds to the centre of vegetation and $x_\ell/(r_\mathrm{s} + r_\mathrm{w}) = \pm 0.5$ corresponds to the centre of the open space between rows. R3.1 (*thick solid line*); R1.1 (*thin solid line*); R3.6 (*thick dashed line*); R1.6 (*thin dashed line*)

only representative canopy geometries are shown. The geometries not shown exhibit the expected behaviour based on the depicted trend. It is important to note that Fig. 12 does not necessary show the spatial probability distribution of structures, but more precisely the spatial proability distribution of pressure spikes that exceeded the specified threshold. The following interpretation assumes that the magnitude of pressure spikes correlates well with turbulence structure strength or coherence. If for a given row-local position there was a high probability of a pressure spike exceeding the threshold, it is probable that coherent structures at that location are also stronger and more coherent. Conversely, if for a given row-local position there was a low probability of a pressure spike exceeding the threshold, it does not necessarily mean that there is a low probability of structures existing in that location, but instead that structures at that location are generally not strong enough to generate a pressure spike that exceeds the threshold.

All horizontally homogeneous canopy cases yielded an approximately uniform distribution in terms of streamwise location of coherent structure trigger events (represented in Fig. 12 by a horizontal dashed line). In cases of small row spacing, pressure spikes that exceeded the threshold have only a small amount of locational preference, where structures were most likely to form within the vegetative row. In cases of large row spacing, trigger events showed high levels of locational preference. Most trigger events occurred just upwind of the vegetative row, and very few events occurred immediately downwind of the row. Particularly in the case of large row spacing, production and development of coherent structures seems to be affected by row heterogeneity. Results suggest that structures are produced at the top of a row and evolve in the wake of vegetation similar to a spatial mixing layer. It is probable that after production near vegetation, structures gain strength and coherence as they evolve downstream of the row, thus resulting in a progressively larger probability of pressure spikes. This is analogous to the coherent structure model commonly associated with isolated windbreaks (Zhuang and Wilson 1994). This interpretation is also supported by the work of Huang et al. (2011), who showed through proper orthogonal decomposition (POD) that the coherence of the flow increases with downwind distance in the wake of a forest-to-clearing transition, which is attributed to the increase in the importance of coherent mixing-layer-like structures. It is probable that this bias in the location of structures has implications on scalar or particle transport in sparse canopies, as this suggests that vertical transport is likely most efficient at the upwind side of a row.

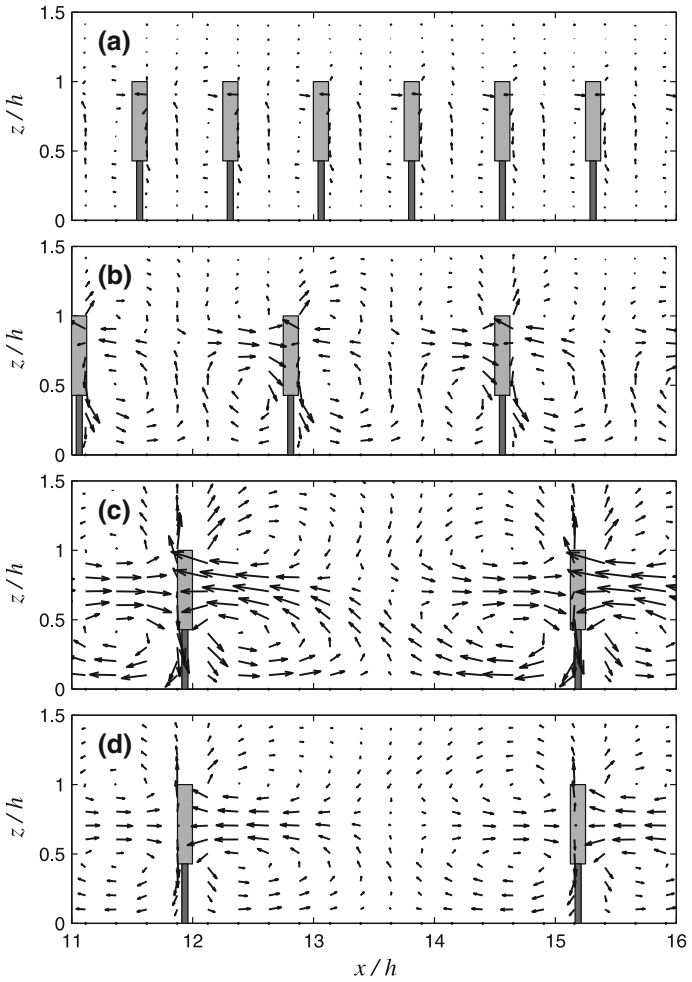

Fig. 13 Spanwise-averaged $\{\overline{u}'', \overline{w}''\}$ vectors for representative canopy geometries. Vectors are drawn to scale, where the maximum vector magnitude is $0.4\,\mathrm{m\,s^{-1}}$. **a** R3.1; **b** R3.3; **c** R3.6; **d** R1.6

3.4.5 Dispersive Flux Structures

Row structure gives contributions to vertical fluxes through standing structures in mean fields. Figure 13 shows spanwise-averaged vectors of $\{\overline{u}'', \overline{w}''\}$ for select row-resolved simulations. These structures form as a result of the drag force imposed at discrete intervals in the streamwise direction. For small row spacing, there is not enough open space to allow the velocity field to recover, or to significantly increase. In canopy geometries with $LAI = 1$, drag as a result of canopy elements is not large enough to cause strong dispersive flux structures to form. However, in cases of large row *LAI* and spacing, strong dispersive flux structures form that can contribute to significant dispersive fluxes.

At the top of the row, high momentum fluid is transported upwards and out of the canopy. This region is likely responsible for the positive dispersive flux observed above the canopy in Fig. 7a. These motions appear to be insignificant in terms of the momentum flux due to the

dominance of the turbulent component of the momentum flux near the canopy top; however these motions may be important for scalar transport near the canopy top. Downwind of the row in the upper half of the canopy, strong ejection motions are present that result in the net negative dispersive flux that was shown in Fig. 7a.

Below a height of $z/h \approx 0.75$, high momentum fluid upwind of the row is transported downward, contributing to a negative dispersive flux. These motions continue downwind of the trunk-space transporting high momentum fluid downwind of the row downward and through the row trunk space. These strong sweeping motions are responsible for the large negative dispersive flux in the lower half of the canopy observed in Fig. 7a. Near the wall, strong Q3 motions just upwind of the row contribute to the net positive dispersive flux, which acts to suppress the momentum flux near the wall.

It is important to note that the vectors shown in Fig. 13 correspond to velocity fluctuations, and thus do not include mean advection. Although recirculation zones appear in Fig. 13, horizontal advection still dominates streamwise transport and no recirculation zone exists in the actual flow (i.e., $\overline{u} > 0$). This is in contrast to many forest-to-clearing transition studies that report a pronounced recirculation zone (Cassiani et al. 2008; Huang et al. 2011). However, it is expected that a sufficient increase in row *LAI* or decrease in U would result in a recirculation zone, as suggested by many studies examining flow around windbreaks (Plate 1971).

The discussion of canopy structures is concluded by mentioning that there were no noticeable effects of domain size on both types of structures just discussed. This suggests that these near-canopy structures are not directly affected by larger outer-layer structures.

4 Summary

A LES study was performed to examine flow in structured sparse canopies. The focus was to determine how plane-averaged turbulence statistics and the local structure of turbulence were affected by canopy heterogeneity. The model canopy consisted of a set of infinitely repeating rows of vegetation oriented perpendicular to the mean wind direction. To illustrate the effects of heterogeneity, row spacing and *LAI* were varied. Simulations were performed for row *LAI* ranging from 1.0 to 3.0 and row spacings ranging from 1.0 to 6.0 m. To assess the impacts of canopy heterogeneity, results were contrasted with horizontally homogeneous canopies that are equivalent in terms of their overall or effective leaf area index.

In general, the effects of canopy heterogeneity were largest in geometries with large row *LAI* and spacing. Profiles of velocity moments showed that the effects of heterogeneity were most significant for higher-order moments, while first-order moments (i.e., mean values) showed good agreement between the row-resolved and homogeneous canopies indicating an insensitivity to canopy heterogeneity. From a modelling perspective, this indicates that horizontal canopy heterogeneity should not have to be explicitly included to accurately approximate the mean flow for the canopy geometries examined here. The skewness of the vertical velocity component showed that the horizontally homogeneous canopy representation substantially underestimated skewness within the canopy in cases of large row *LAI* and spacing, which was seen as a potential indicator for underlying differences in turbulence structure. The horizontally homogeneous canopy representation underestimated the normalized turbulent momentum flux by as much as 50 % near $z/h = 0.5$, indicating that heterogenity has a significant effect on vertical turbulent transport in the lower canopy. The horizontally homogeneous canopy representation also underestimated the total momentum flux (sum of turbulent and dispersive components) by up to

an additional 20 % as a result of dispersive fluxes, which were largest near mid-canopy height. Differences between the row-resolved and horizontally homogeneous canopies are attributed in part to large open spaces in the heterogeneous canopy. This can cause significant local flow accelerations as the flow starts to recover to its freestream state and then abruptly impacts upon dense vegetation similar to that of a set of repeating windbreaks.

An additional mechanism behind the differences in higher-order velocity moments for the two canopy representations is likely that the nature of turbulent structure production and development is inherently different. In the horizontally homogeneous canopy, the mixing-layer-like structures are produced in a similar way as a planar mixing layer. The spatial distribution of turbulent structures is quasi-uniform, with no spatial preference for the existence of structures. However, in the case of the highly heterogeneous canopy, structures seem to be produced off the leeward edge of the top of the row, similar to that of a spatially developing mixing layer behind a splitter plate. This model for structure production and development is also analogous to the model commonly presented for isolated windbreaks (Zhuang and Wilson 1994). This idea is supported by the fact that, using the detection method of Finnigan et al. (2009), the frequency of detected structures for a given threshold tends to increase downwind of vegetative rows. This may have important implications for scalar transport in sparse canopies, as it appears that the most efficient vertical turbulent transport is likely to occur just upwind of the rows.

Despite the differences in the coherent structure production mechanisms between the heterogeneous and homogeneous canopies, we identify similar structures and find that the general nature of turbulence is similar. By examining profiles of vertical velocity skewness and the ratio of Q2 to Q4 contributions to the momentum flux, it appears that the structure of turbulence resembles a mixing layer much more than a pure boundary layer even in the sparsest canopies considered in this study. Furthermore, using the method of Finnigan et al. (2009), we can readily identify very similar coherent structures in both the heterogeneous and homogeneous canopies. Surely the transition from a canopy layer to a rough-wall boundary layer must occur at some canopy density. However, we conclude that there is a wide range of sparse canopies that behave predominantly as a canopy layer, although integral length scales calculated at the canopy top do not follow mixing-layer scaling. This is attributed to integral length scales at the canopy top being poor indicators of length scales associated with mixing-layer-like structures.

Superposed on these coherent turbulent structures in the heterogeneous canopy are dispersive flux structures. These are standing wave-like motions observed in temporally-averaged fields. These structures are responsible for the dispersive fluxes and have the potential to considerably increase total momentum fluxes. Results indicated that, on average, these structures tended to transport momentum up and out of the canopy in the upper third of the canopy, and down into the trunk space in the lower two-thirds of the canopy. By definition, these structures are not present in a truly horizontally homogeneous canopy, and thus this mode of momentum transport is absent. The absence of dispersive fluxes in the homogeneous canopy representation resulted in a reduction in the total momentum flux (sum of turbulent and dispersive components) by over 20 % in the lower canopy when row *LAI* and spacing were large. In contrast, dispersive fluxes were negligible in the cases of $LAI = 1.0$, and in the upper canopy for all geometries.

Acknowledgments This research was partially supported by the University of Utah Research Foundation and National Science Foundation grant IDR CBET-PDM 113458. An allocation of computer time from the Center for High Performance Computing at the University of Utah is gratefully acknowledged.

References

Albertson JD, Parlange MB (1999) Surface length scales and shear stress: implications for land–atmosphere interactions over complex terrain. Water Resour Res 35:2121–2132

Amiro BD (1990) Drag coefficients and turbulence spectra within three boreal forest canopies. Boundary-Layer Meteorol 52:227–246

Baldocchi DD, Hutchinson BA (1987) Turbulence in an almond orchard: vertical variation in turbulence statistics. Boundary-Layer Meteorol 40:127–146

Böhm M, Finnigan JJ, Raupach MR (2000) Dispersive fluxes and canopy flows: just how important are they? In: 24th symposium on agricultural and forest meteorology, vol 5(5), pp 106–107

Bohrer G, Katul GG, Walko RL, Avissar R (2009) Exploring the effects of microscale structural heterogeneity of forest canopies using large-eddy simulations. Boundary-Layer Meteorol 132:351–382

Brunet Y, Finnigan JJ, Raupach MR (1994) A wind tunnel study of air flow in waving wheat: single-point velocity statistics. Boundary-Layer Meteorol 70:95–132

Calaf M, Meneveau C, Meyers J (2010) Large eddy simulation study of fully developed wind-turbine array boundary layers. Phys Fluids 22(015):110

Canuto C, Hussaini MY, Qaurteroni A, Zang TA (1988) Spectral methods in fluid dynamics. Springer, New York

Cassiani M, Katul GG, Albertson JD (2008) The effects of canopy leaf area index on airflow across forest edges: large-eddy simulation and analytical results. Boundary-Layer Meteorol 126:433–460

Cava D, Katul GG (2008) Spectral short-circuiting and wake production within the canopy trunk space of and alpine hardwood forest. Boundary-Layer Meteorol 126:415–431

Cescatti A, Marcolla B (2004) Drag coefficient and turbulence intensity in conifer canopies. Agric For Meteorol 121:197–206

Cheng H, Castro IP (2002) Near wall flow over urban-like roughness. Boundary-Layer Meteorol 104:229–259

Chester S, Meneveau C, Parlange MB (2007) Modeling turbulent flow over fractal trees with renormalized numerical simulation. J Comp Phys 225:427–448

Christen A, Vogt R (2004) Direct measurement of dispersive fluxes within a cork oak plantation. In: Proceedings of 26th conference on agricultural and forest meteorology. American Meteorological Society, Vancouver

Dupont S, Brunet Y (2008) Influence of foliar density profile on canopy flow: a large-eddy simulation study. Agric For Meteorol 148:976–990

Dwyer MJ, Patton EG, Shaw RH (1997) Turbulent kinetic energy budgets from a large-eddy simulation of airflow above and within a forest canopy. Boundary-Layer Meteorol 84:23–43

Finnigan JJ (2000) Turbulence in plant canopies. Annu Rev Fluid Mech 32:519–571

Finnigan JJ, Shaw RH (2000) A wind tunnel study of airflow in waving wheat: an EOF analysis of the structure of the large-eddy motion. Boundary-Layer Meteorol 96:211–255

Finnigan JJ, Shaw RH (2008) Double-averaging methodology and its application to turbulent flow in and above vegetation canopies. Environ Sci Technol 56:534–561

Finnigan JJ, Shaw RH, Patton EG (2009) Turbulence structure above a vegetation canopy. J Fluid Mech 637:387–424

Fitzmaurice L, Shaw RH, Paw UKT, Patton EG (2004) Three-dimensional scalar microfront systems in a large-eddy simulation of vegetation canopy flow. Boundary-Layer Meteorol 112:107–127

Gladstone EA, Dokoozlian NK (2003) Influence of leaf area density and trellis/training system on light microclimate within grapevine canopies. Vitis 42:123–131

Huang J, Cassiani M, Albertson JD (2009) The effects of vegetation density on coherent turbulent structures within the canopy sublayer: a large-eddy simulation study. Boundary-Layer Meteorol 133:253–275

Huang J, Cassiani M, Albertson JD (2011) Coherent turbulent structures across a vegetation density. Boundary-Layer Meteorol 140:1–22

Jackson PS (1981) On the displacement height in the logarithmic velocity profile. J Fluid Mech 111:15–25

Johnson LF, Roczen DE, Youkhana SK, Nemani RR, Bosch DF (2003) Mapping vineyard leaf area with multispectral satellite imagery. Comput Electron Agric 38:33–44

Judd MJ, Raupach MR, Finnigan JJ (1996) A wind tunnel study of turbulent flow around single and multiple windbreaks, Part I: velocity fields. Boundary-Layer Meteorol 80:127–165

Kaimal JC, Finnigan JJ (1994) Atmospheric boundary layer flows: their structure and measurement. Oxford University Press, New York, 289 pp

Kanda M, Hino M (1994) Organized structures in developing turbulent flow within and above a plant canopy, using a large eddy simulation. Boundary-Layer Meteorol 68:237–257

Lauri PE (2009) Developing a new paradigm for apple training. Compact Fruit Tree 42:17–19

Lu SS, Willmarth WW (1973) Measurements of the structure of Reynolds stress in a turbulent boundary layer. J Fluid Mech 60:481–571

Mason PJ, Callen NS (1986) On the magnitude of the subgrid-scale eddy coefficient in large-eddy simulations of turbulent channel flow. J Fluid Mech 162:439–462
McAneney KJ, Judd MJ (1991) Multiple windbreaks: an aeolean ensemble. Boundary-Layer Meteorol 54: 129–146
Novak MD, Warland JS, Orchansky AL, Ketler R, Green S (2000) Wind tunnel and field measurements of turbulent flow in forests, Part I: uniformly thinned stands. Boundary-Layer Meteorol 95:457–495
Patton EG, Shaw RH, Paw U KT, Moeng CH (1994) A comparison of two large-eddy simulations of turbulent flow above and within a forest canopy. In: 21st conference on agriculture and forest meteorology, vol 4(7), pp 88–91
Patton EG, Shaw RH, Paw U KT (1995) Large-eddy simulation of a forest: Influence of canopy structure on turbulent kinetic energy. In: 11th symposium on boundary layers and turbulence, vol 15(2), pp 525–528
Patton EG, Shaw RH, Judd MJ, Raupach MR (1998) Large-eddy simulation of windbreak flow. Boundary-Layer Meteorol 87:275–306
Patton EG, Sullivan PP, Davis KJ (2003) The influence of a forest canopy on top-down and bottom-up diffusion in the planetary boundary layer. Q J R Meteorol Soc 129:1415–1434
Plate EJ (1971) The aerodynamics of shelter belts. Agric Meteorol 8:203–222
Poggi D, Katul GG (2008) Micro- and macro-dispersive fluxes in canopy flows. Environ Sci Technol 56: 778–800
Poggi D, Porporato A, Ridolfi L, Albertson JD, Katul GG (2004a) The effect of vegetation density on canopy sub-layer turbulence. Boundary-Layer Meteorol 111:565–587
Poggi D, Porporato A, Ridolfi L, Albertson JD, Katul GG (2004b) Interaction between large and small scales in the canopy sublayer. Geophys Res Lett 31:L05,102
Pope S (2000) Turbulent flows. Cambridge University Press, UK, 771 pp
Raupach MR, Shaw RH (1982) Averaging procedures for flow within vegetation canopies. Boundary-Layer Meteorol 22:79–90
Raupach MR, Finnigan JJ, Brunet Y (1996) Coherent eddies and turbulence in vegetation canopies: the mixing-layer analogy. Boundary-Layer Meteorol 78:351–382
Reynolds RT, Hayden P, Castro IP, Robins AG (2007) Spanwise variations in nominally two-dimensional rough-wall boundary layers. Exp Fluids 42:311–320
Robinson SK (1991) Coherent motions in the turbulent boundary layer. Annu Rev Fluid Mech 23:601–639
Schlegel F, Stiller J, Bienert A, Maas HG, Queck R, Bernhofer C (2012) Large-eddy simulation of inhomogeneous canopy flows using high resolution terrestrial laser scanning data. Boundary-Layer Meteorol 142:223–243
Shaw RH (1977) Secondary wind speed maxima inside plant canopies. J Appl Meteorol 16:514–521
Shaw RH, Patton EG (2003) Canopy element influences on resolved- and subgrid-scale energy within a large-eddy simulation. Agric For Meteorol 115:5–17
Shaw RH, Schumann U (1992) Large-eddy simulation of turbulent flow above and within a forest. Boundary-Layer Meteorol 61:47–64
Shaw RH, Brunet Y, Finnigan JJ, Raupach MR (1995) A wind tunnel study of air flow in waving wheat: two-point velocity statistics. Boundary-Layer Meteorol 76:349–376
Stoll R, Porté-Agel F (2006a) Dynamic subgrid-scale models for momentum and scalar fluxes in large-eddy simulations of neutrally stratified atmospheric boundary layers over heterogeneous terrain. Water Resour Res 42:W01,409
Stoll R, Porté-Agel F (2006b) Effect of roughness on surface boundary conditions for large-eddy simulation. Boundary-Layer Meteorol 118:169–187
Stoll R, Porté-Agel F (2008) Large-eddy simulation of the stable atmospheric boundary layer using dynamic models with different averaging schemes. Boundary-Layer Meterology 126:1–28
Stoll R, Porté-Agel F (2009) Surface heterogeneity effects on regional-scale fluxes in stable boundary layers: surface temperature transitions. J Atmos Sci 66(2):412–431
Stull RB (1988) An introduction to boundary layer meteorology. Kluwer, Dordrecht, 670 pp
Su HB, Schmid HP, Vogel CS, Curtis PS (1998) Effects of canopy morphology and thermal stability on mean flow and turbulence statistics observed inside a mixed hardwood forest. Boundary-Layer Meteorol 88:363–397
Talaie A, Shojaie-Saadee M, Dadashpur A, Asgari-Sarcheshmeh M (2011) Fruit quality in five apple cultivars trees trained to intensive training system: Geneva y-trellis. Genetika 43:153–161
Tarara J, Ferguson J, Hoheisel G (2005) Asymmetrical canopy architecture due to prevailing wind direction and row orientation creates an imbalance in irradiance at the fruiting zone in grapevines. Agric For Meteorol 135:144–155
Thom AS (1968) The exchange of momentum, mass and heat between an artificial leaf and airflow in a wind tunnel. Q J R Meteorol Soc 94:44–55

Thom AS (1971) Momentum absorption by vegetation. Q J R Meteorol Soc 97:414–428
Thomas C, Foken T (2007) Flux contribution of coherent structures and its implications for the energy and matter in a tall spruce canopy. Boundary-Layer Meteorol 123:317–337
Townsend AA (1976) The structure of turbulent shear flow, 2nd edn. Cambridge University Press, UK, 442 pp
van Hout RE (2007) PIV measurements in the atmospheric boundary layer within and above a mature corn canopy, Part I: statistics and energy flux. J Atmos Sci 64:2805–2824
Wan F, Porté-Agel F, Stoll R (2007) Evaluation of dynamic subgrid-scale models in large-eddy simulations of neutral flow over a two-dimensional sinusoidal hill. Atmos Environ 41:2719–2728
Wang H, Takle ES (1995) Boundary-layer flow and turbulence near porous obstacles. Boundary-Layer Meteorol 74:73–88
Watanabe T (2004) Large-eddy simulation of coherent turbulence structures associated with scalar ramps over plant canopies. Boundary-Layer Meteorol 112:307–341
Wilson JD (1985) Numerical studies of flow through a windbreak. J Wind Eng Ind Aerodyn 21:119–154
Wilson JD, Yee E (2003) Calculation of winds disturbed by an array of fences. Agric For Meteorol 115:31–50
Yang B, Raupach MR, Shaw RH, Paw UKT, Morse AP (2006a) Large-eddy simulation of turbulent flow across a forest edge, Part I: flow statistics. Boundary-Layer Meteorol 120:377–412
Yang B, Morse AP, Shaw RH, Paw UKT (2006b) Large-eddy simulation of turbulent flow across a forest edge. Part II: momentum and kinetic energy budgets. Boundary-Layer Meteorol 121:433–457
Yi C (2007) Momentum transfer within canopies. J Appl Meteorol Clim 47:262–275
Yue W, Parlange MB, Meneveau C, Zhu W, van Hout R, Katz J (2007) Large-eddy simulation of plant canopies using plant-scale representation. Boundary-Layer Meteorol 124:183–203
Zhou J, Adrian RJ, Balachandar S, Kendall TM (1999) Mechanisms for generating coherent packets of hairpin vortices in channel flow. J Fluid Mech 387:353–396
Zhuang Y, Wilson JD (1994) Coherent motions in windbreak flow. Boundary-Layer Meteorol 70:151–169